

Theory and Design of Two-Dimensional Filter Banks: A Review

YUAN-PEI LIN

Department of Electrical Engineering, 136-93, California Institute of Technology, Pasadena, CA 91125

P. P. VAIDYANATHAN

ppvnath@sys.caltech.edu

Department of Electrical Engineering, 136-93, California Institute of Technology, Pasadena, CA 91125

Abstract. There has been considerable interest in the design of multidimensional (MD) filter banks. MD filter banks find application in subband coding of images and video data. MD filter banks can be designed by cascading one-dimensional (1D) filter banks in the form of a tree structure. In this case, the individual analysis and synthesis filters are separable and the filter bank is called a separable filter bank. MD filter banks with nonseparable filters offer more flexibility and usually provide better performance. Nonetheless, their design is considerably more difficult than separable filter banks. The purpose of this paper is to provide an overview of developments in this field on the design techniques for MD filter banks, mostly two-dimensional (2D) filter banks. In some image coding applications, the 2D two-channel filter banks are of great importance, particularly the filter bank with diamond-shaped filters. We will present several design techniques for the 2D two-channel nonseparable filter banks. As the design of MD filters are not as tractable as that of 1D filters, we seek design techniques that do not involve direct optimization of MD filters. To facilitate this, transformations that turn a separable MD filter bank into a nonseparable one are developed. Also, transformations of 1D filter banks to MD filter banks are investigated. We will review some designs of MD filter banks using transformations. In the context of 1D filter bank design, the cosine modulated filter bank (CMFB) is well-known for its design and implementation efficiency. All the analysis filters are cosine modulated versions of a prototype filter. The design cost of the filter bank is equivalent to that of the prototype and the implementation complexity is comparable to that of the prototype plus a low-complexity matrix. The success with 1D CMFB motivate the generalization to the 2D case. We will construct the 2D CMFB by following a very close analogy of 1D case. It is well-known that the 1D lossless systems can be characterized by state space description. In 1D, the connection between the losslessness of a transfer matrix and the unitariness of the realization matrix is well-established. We will present the developments on the study of 2D lossless systems. As in 1D case, the 2D FIR lossless systems can be characterized in terms of state space realizations. We will review this, and then address the factorizability of 2D FIR lossless systems by using the properties of state space realizations.

1. Introduction

One-dimensional (1D) filter banks have been shown to be very useful in subband coding applications. The typical applications of 1D filter banks are in the coding of speech and music [55]. For multidimensional (MD) filter banks, applications include coding and compression of images and video data. Consider the filter bank in Fig. 1.1. Two of the basic building blocks are the decimator \mathbf{M} and the expander \mathbf{M} . In 1D systems, the M -fold decimator keeps only the samples that are multiples of M . In D -dimensional systems, the decimator \mathbf{M} is a $D \times D$ nonsingular integer matrix. The decimation matrix \mathbf{M} keeps those samples that are on the lattice generated by \mathbf{M} . The lattice generated by an integer matrix \mathbf{M} is the set of integer vectors of the form

$$\mathbf{M}\mathbf{d}, \quad \text{for some } D \times 1 \text{ integer vector } \mathbf{d}.$$

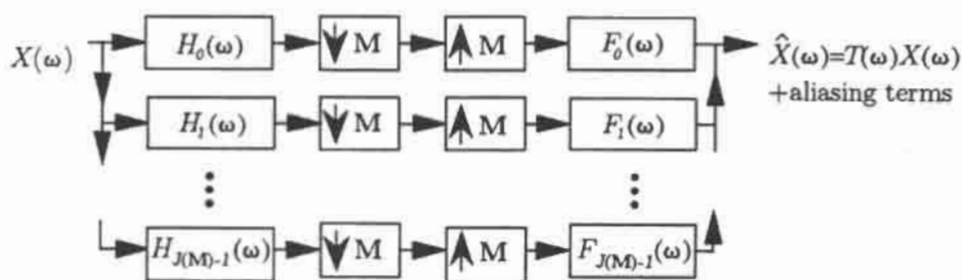
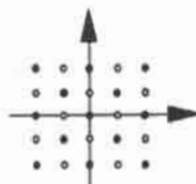


Figure 1.1. $J(M)$ -channel maximally decimated filter bank, where $J(M) = |\det \mathbf{M}|$.



- Integers
- Integers on lattice of \mathbf{Q}

Figure 1.2. The lattice generated by \mathbf{Q} , the quincunx lattice.

For example, let \mathbf{M} be the quincunx matrix \mathbf{Q} defined as

$$\mathbf{Q} = \begin{pmatrix} 1 & 1 \\ -1 & 1 \end{pmatrix}. \quad (1.1)$$

The lattice of \mathbf{Q} is as shown in Fig. 1.2 and is called the quincunx lattice. The output of the decimator \mathbf{Q} contains only the samples on the lattice of \mathbf{Q} . Suppose the system in Fig. 1.1 has input $X(\mathbf{z})$, then the output of the filter bank $\hat{X}(\mathbf{z})$ consists of $X(\mathbf{z})T(\mathbf{z})$ and some aliasing terms. When the output is free from aliasing error, the system is LTI with transfer function $T(\mathbf{z})$, called the distortion function. If $T(\mathbf{z})$ is a delay, the alias-free filter bank is said to have perfect reconstruction.

The simplest way to design MD filter banks is to cascade 1D filter banks in the form of a tree structure. In these tree-structured filter banks, the decimation matrix \mathbf{M} is diagonal and data is processed in each dimension separately. This type of systems is referred to as separable. For a D dimensional separable filter bank, design cost is equivalent to D times that of 1D filter banks; complexity of design and implementation grows linearly with the number of dimensions. However, in this case, the supports of the analysis and synthesis filter are D -dimensional rectangles, e.g., rectangles in two-dimensional (2D) case. In nonseparable filter banks, the supports of the analysis and synthesis filters could

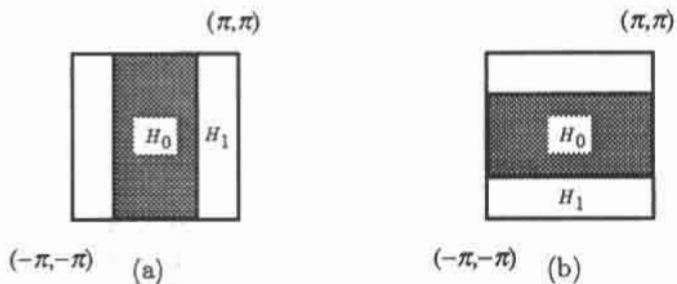


Figure 1.3. Two types of support configurations for separable two-channel filter banks.

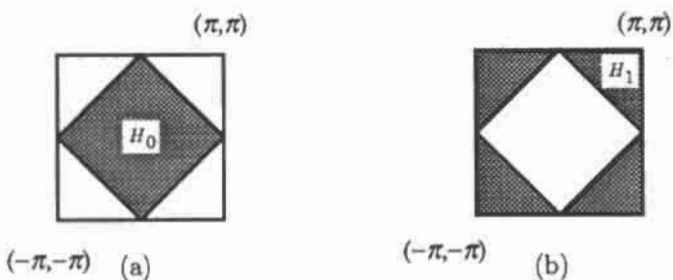


Figure 1.4. The support configuration of the diamond filter bank. (a) The lowpass analysis and synthesis filters. (b) The highpass analysis and synthesis filters.

have a variety of shapes, e.g., parallelepipeds that are not rectangles. Usually different support configurations are desired for different applications. For example, consider 2D two-channel systems. If we use a separable system, the support configuration will be as in Fig. 1.3(a) or Fig. 1.3(b) when the analysis and synthesis filters have real coefficients. (The analysis and the synthesis filters typically have the same supports; only the supports of the analysis filters are shown.) Because the human eye is less sensitive to high frequency component, in some applications of image coding it is desired that one subband has as much low frequency information as possible. For these applications, a support configuration as shown in Fig. 1.4 might yield better results [7]. Due to the shapes of the lowpass filters, this system is termed a diamond filter bank. In directional subband coding applications [3], [30], where directional sensitivity of the filters is important, the use of quadrant filter banks (Fig. 1.5) or filter banks with fan filters (Fig. 1.6) might be preferred. None of these support configurations, diamond, quadrant or fan, can be achieved by separable filter banks. Although nonseparable filter banks offer more flexibility and usually provide better performance, in most cases their design is considerably more difficult than separable filter banks. The implementation complexity of nonseparable filter banks is usually also higher.

Filter banks for the application of subband coding of speech were introduced in the 1970s [12]. Since then, studies on filter banks and subband coding have been booming [1]–[14].

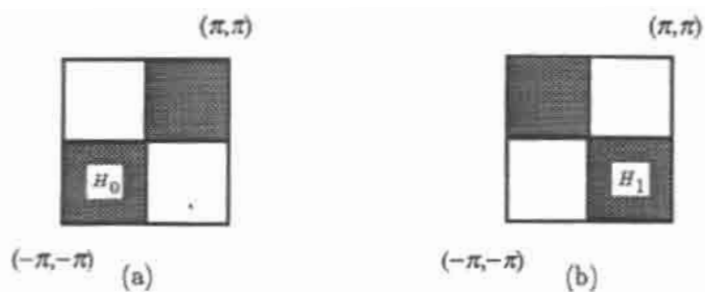


Figure 1.5. The support configuration of the quadrant filter bank. (a) The support of $H_0(\mathbf{w})$. (b) The support of $H_1(\mathbf{w})$.

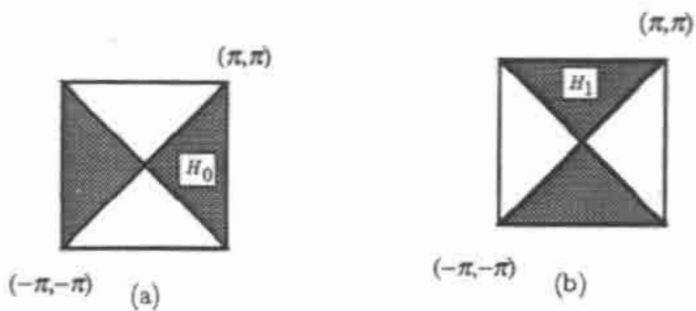


Figure 1.6. The filter bank with fan filters. (a) The support of $H_0(\mathbf{w})$. (b) The support of $H_1(\mathbf{w})$.

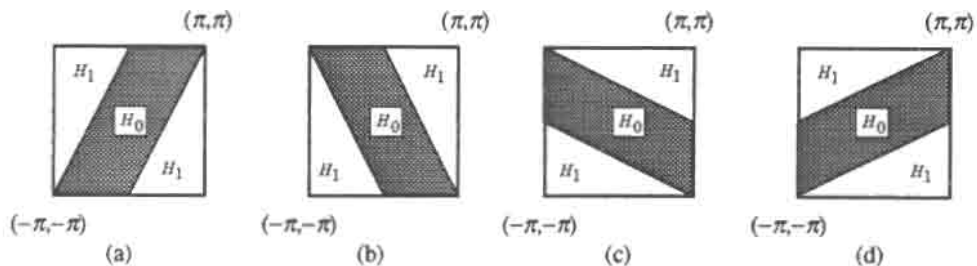


Figure 1.7. Four possible parallelogram supports of the two-channel filter bank.

[17]–[35], [37]–[39], [41]–[55]. Activities in the area of MD filter banks started in 1980s. Some of the earliest contributions were due to Vetterli [52], and Woods and O’Neil [54]. The idea of lattice decimation and expansion is an indispensable aspect of MD multirate systems. An introduction to MD sampling and signal processing can be found in [15]. A more detailed treatment is given in [50]. The theoretical aspects of MD systems are studied in [5]. An excellent tutorial of MD filter banks is given in [53]. Review of fundamentals of MD filter banks can be found at [48], [7], [Chapter 12, 50]. Results on the commutativity of MD decimators and expanders have been reported in [27], [22], [6], [17], [18]. Recently, the relation between filter banks and discrete wavelet transform has been extended to MD case [11], [28], and will not be elaborated in this paper.

1.1. Scope and Overview

The purpose of this paper is to provide an overview of developments on the design of MD filter banks, mostly 2D filter banks. Several design techniques for MD nonseparable filter banks will be discussed in this paper. They are outlined as follows.

1. Two-dimensional two-channel filter banks (Sec. II)

Commonly used 2D two-channel filter banks. Many studies have been done on 2D two-channel filter banks (Fig. 1.1 with $|\det \mathbf{M}| = 2$). In particular, the diamond filter bank (Fig. 1.4), first introduced by Vetterli [52], is of special interest in some image coding applications. The decimation matrix \mathbf{M} for the diamond filter bank is usually the quincunx matrix \mathbf{Q} as in (1.1). There is also some interest in the filter bank with quadrant filters as shown in Fig. 1.5, [3], [30], [45]. The support of $H_0(\mathbf{z})$ is in quadrants I and III while the support of $H_1(\mathbf{z})$ is in quadrants II and IV. Filter banks in which the filters have parallelogram supports are of importance in some applications [3]. Several possible parallelogram supports for the analysis and synthesis filters are shown in Fig. 1.7. The filter bank with fan filters (Fig. 1.6) is closely related to the diamond filter bank. From Fig. 1.6, we see that the fan filters can be obtained by shifting the diamond filters by $(\pi \ 0)^T$ in frequency domain.

Design of the diamond filter bank. Most of the design techniques for 2D two-channel systems are developed for the diamond filter bank. For the two-channel systems, there are only four filters, two analysis filters and two synthesis filters. So in some designs, two (or three) of the four filters are chosen such that the system is alias free. The remaining two (or one) filters are then optimized to achieve approximate reconstruction [3], [52] or perfect reconstruction [1], [2], [24], [38], [45]. As 2D filters are considerably more difficult to design than 1D filters, in many cases (approximate reconstruction or perfect reconstruction) the 2D filters are obtained from 1D filters by appropriate mappings [1–3], [24], [38], [45]. In [2], Ansari and Lau proposed a design technique for the perfect reconstruction diamond filter bank. A polyphase mapping method is proposed therein to design IIR analysis filters. For filter banks with FIR filters, several 1D to 2D transformations have been considered. For example, the McClellan transformation is used in [1]. In [45], a more general transformation is considered and the design technique can be used for the diamond filter bank, the quadrant filter bank or filter banks with other types of supports. More recently [24], [38], a polyphase mapping similar to that in [2] is used to design a diamond filter bank. This technique allows the use of FIR or IIR filters, and moreover, in the IIR case the filters are guaranteed to be causal and stable.

Design of other types of filter banks. The design of the other commonly used filter banks is closely related to that of the diamond filter bank. The fan filters (Fig. 1.6) are shifted versions of the diamond filters and hence can be obtained by first designing the diamond filter bank. The filter banks in which the filters have parallelogram supports (Fig. 1.7) can be derived from the diamond filter bank by using the so-called unimodular transformation. This will be addressed in Sec. III. Some of the design techniques developed for the diamond filter bank [24], [38], [45], can be applied to the quadrant filter bank (Fig. 1.5) with some modifications.

In Sec. II, we will review two design techniques for the diamond filter bank. The first one proceeds along the line of [1] and the second one proceeds along the line of [24], [38]. A design example of the diamond filter bank through the second approach is also given in Sec. II. Although the design of quadrant filter banks (Fig. 1.5) is not mentioned in these references, we will see that the generalization to quadrant filter banks can be achieved easily.

2. Designs of MD multiple channel filter banks using transformations (Sec. III)

As MD nonseparable filter banks are considerably more difficult to design than 1D filter banks, various 1D to MD transformations have been proposed for designing suboptimal MD filter banks without actually optimizing MD filters. In the design of two-channel 2D filter banks (Sec. II), we will see such examples. For filter banks with more than two channels, two types of transformation have been proposed. In [49], the so-called unimodular transformation is developed. By use of the unimodular transformation, we can convert a MD separable filter bank to a nonseparable one. Consider a D -dimensional M -channel filter bank with separable filters. Applying unimodular transformation on the separable system, the new filter bank is still D -dimensional and has M channels, but the new analysis

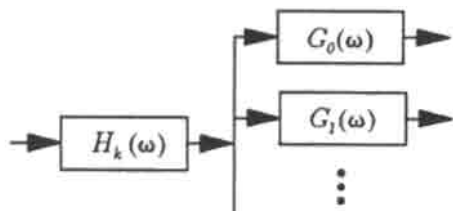


Figure 1.8. Tree structured analysis filter bank. Splitting of the k th subband.

and synthesis filters are nonseparable. Using the unimodular transformation, we will see that the 2D two-channel filter banks with parallelogram-supported filters (Fig. 1.7) can be derived from the diamond filter bank. In [43], Shah and Kalker studied transformations of 1D filter banks to D -dimensional filter banks. They proposed a 1D to D -dimensional transformation that preserves perfect reconstruction. We will present a review of these two transformations in Sec. III.

3. Tree-structured filter banks (Sec. IV)

Given an analysis filter bank, suppose we take a particular subband and split it into further subbands as shown in Fig. 1.8. By repeating this operation, we can actually build up a tree structured analysis bank. The most common example of a 1D tree structured filter bank is the one that results in an octave stacking of the passbands. In the 2D case, tree structures based on simple two-channel modules can offer sophisticated band-splitting schemes (sophisticated supports), especially if we combine the various configurations in Fig. 1.4–Fig. 1.7 appropriately. The directional filter bank developed by Bamberger and Smith (Fig. 1.9) is such an example [3]. We will review a number of tree structure examples in Sec. IV.

4. Two-dimensional cosine modulated filter bank (Sec. V–VII)

The one-dimensional (1D) cosine modulated filter bank (CMFB) has been studied extensively in the past [10], [41], [37], [39], [35], [26]. In the 1D CMFB, each analysis and synthesis filter is a cosine modulated version of one or two prototype filters. The CMFB has the advantages of low design cost and low implementation complexity. The success with 1D CMFB motivates the construction of 2D CMFB [19], [20], [29], [32], [31]. The separable 2D CMFB can always be obtained through concatenation of two 1D CMFB by using a tree structure. Our interest here is in designing a nonseparable 2D CMFB. The prototype filter is in general a nonseparable 2D FIR filter with a parallelogram support. Each analysis and synthesis filter is a cosine modulated version of the prototype, and is also nonseparable. In the separable 2D CMFB case, each individual filter consists of four shifts of a separable 2D prototype. However, the real-coefficient constraint on the analysis filter

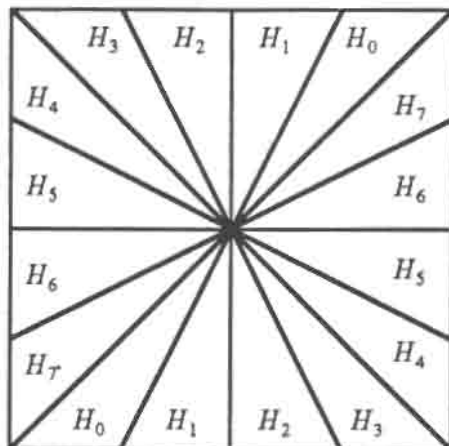


Figure 1.9. Supports of the analysis filters in the directional filter bank.

requires only two copies of the prototype. We can conceive that in the more general 2D CMFB the analysis filters can have two or four shifted copies of the prototype. So we will consider two classes of 2D FIR paraunitary cosine modulated filter banks: the two-copy CMFB and the four-copy CMFB. In the two-copy CMFB, each analysis filter contains two copies of the prototype and in the four-copy CMFB, each analysis filter contains four copies of the prototype. The filter bank will eventually be constrained to be paraunitary; the synthesis filters have the same support as the corresponding analysis filters.

The construction of the two-copy CMFB is analogous to the construction of 1D CMFB. For a filter bank with decimation matrix \mathbf{M} , non-diagonal in general, we start from a uniform 2D DFT filter bank with twice the number of channels. All the filters in the DFT filter bank is a shifted version of a prototype filter, which has a parallelogram support. The filters in the DFT filter bank are shifted and then paired to obtain real-coefficient analysis filters. Each analysis filter consists of two copies of the prototype and is a cosine modulated version of the prototype. We then study how to cancel major aliasing and constrain the prototype to ensure perfect reconstruction of the two-copy CMFB.

The four-copy CMFB will be constructed in a similar way. But in the four-copy case, we start from a uniform DFT filter bank with four times the number of channels. Then we shift the filters in the DFT filter bank and combine four shifted filters to obtain real-coefficient analysis filters. Necessary conditions on the decimation matrix will be derived for cancellation of major aliasing.

5. Two-dimensional FIR lossless systems (Sec. VIII)

In a M -channel paraunitary filter bank, the polyphase matrix of the analysis bank $\mathbf{E}(z)$ is paraunitary, [50]. If in addition to being paraunitary, $\mathbf{E}(z)$ is causal and stable, we

say $E(z)$ is lossless. Lossless matrices play an important role in the study and design of paraunitary systems. The 1D FIR lossless systems have been studied extensively in the past. It is known that 1D causal rational systems can be described by state space description. Moreover, the 1D FIR lossless systems can be characterized in terms of state space realization. The connection between the losslessness of the transfer matrix and the unitariness of the realization matrix is well-established [46], [50]. This connection also forms the basis for the factorization result developed in [14]. It is shown therein that the class of 1D FIR lossless systems can be factorized into some basic building blocks. To be more specific, we need to introduce the notion of degree for causal systems. Let $E(z)$ be a causal system, then its degree is the minimum number of delay units (i.e., z^{-1}) required to implement $E(z)$. It is shown in [14] that, all the 1D FIR lossless systems can be expressed as a product of a unitary matrix and degree-one building blocks. Similar approach can be attempted in the 2D case, but the details are more involved. An extensive study has been made by Venkataraman and Levy [51] and independently by Basu, Choi, and Chiang [4]. In Sec. VIII we will review some of the results in [51], [4].

1.2. Paper Outline and Notations

Paper outline. This paper is organized as follows: Sec. II is devoted to the designs of 2D two-channel filter banks, particularly the diamond filter bank and the quadrant filter bank. In Sec. III, we discuss the design of MD filter banks by using transformations. Some useful special cases of tree-structured filter banks are given in Sec. IV. In Sec. V, we introduce the two-copy CMFB and four-copy CMFB. Several issues that arise in the design of 2D CMFB will also be addressed. Details of two-copy CMFB and four-copy CMFB are given respectively in Sec. VI and VII. Developments in the study of 2D FIR lossless systems are presented in Sec. VIII. We will see the characterization of 2D FIR lossless systems in terms of state space realization. Factorizability of 2D FIR lossless systems will also be discussed in Sec. VIII. Except for the results presented in Sec. III, all the design techniques discussed in this paper are developed for 2D systems.

Notations. Notations in this paper are as in [50]. In particular, we will use the following notations.

- (a) Boldfaced lower case letters are used to represent vectors and boldfaced upper case letters are reserved for matrices. The notations \mathbf{A}^T , \mathbf{A}^* , and \mathbf{A}^\dagger represent the transpose, conjugate, and transpose-conjugate of \mathbf{A} . The 'tilde' notation is defined as follows: $\tilde{\mathbf{A}}(z) = \mathbf{A}^\dagger(1/z^*)$.
- (b) When a function has vector argument, e.g. $P(\mathbf{z})$, $\mathbf{z} = (z_0 \ z_1 \ \dots \ z_{D-1})^T$, we will use $P(\mathbf{z})$ and $P(z_0 \ z_1 \ \dots \ z_{D-1})$ interchangeably.
- (c) The notation \mathbf{I}_k denotes a $k \times k$ identity matrix, and the subscript will be omitted when it is clear from the context.

1.3. Summary of Integer Matrices and Multirate Systems

Fundamentals of integer matrices and multirate systems can be found in [7], [48], [50], [53]. A summary is given below.

1.3.1. Fundamentals of integer matrices

1. *Unimodular matrix.* An integer matrix \mathbf{U} is unimodular if $|\det \mathbf{U}| = 1$.
2. *The notations $\mathcal{N}(\mathbf{M})$, $J(\mathbf{M})$ and $SPD(\mathbf{M})$.* Let \mathbf{M} be a $D \times D$ nonsingular integer matrix. The notation $\mathcal{N}(\mathbf{M})$ is defined as the set of integer vectors of the form $\mathbf{M}\mathbf{x}$, where $\mathbf{x} \in [0, 1)^D$. The number of elements in $\mathcal{N}(\mathbf{M})$ is denoted by $J(\mathbf{M})$, which is equal to $|\det \mathbf{M}|$. In 1D case $D = 1$, and $\mathcal{N}(\mathbf{M}) = \{0, 1, 2, \dots, \mathbf{M} - 1\}$. The symmetric parallelepiped $SPD(\mathbf{M})$ is defined as $SPD(\mathbf{M}) = \{\mathbf{M}\mathbf{x}, \mathbf{x} \in [-1, 1)^D\}$.
3. *Division theorem for integer vectors.* Let \mathbf{M} be a $D \times D$ matrix and \mathbf{n} be a $D \times 1$ integer vector. We can express \mathbf{n} as $\mathbf{n} = \mathbf{n}_0 + \mathbf{M}\mathbf{k}$, $\mathbf{n}_0 \in \mathcal{N}(\mathbf{M})$. Moreover, \mathbf{n}_0 and \mathbf{k} are unique. This relation is denoted by $\mathbf{n} = \mathbf{n}_0 \bmod \mathbf{M}$.
4. *Lattices.* The lattice generated by an integer matrix \mathbf{M} is denoted by $LAT(\mathbf{M})$.
5. *The Smith form.* A $D \times D$ integer matrix \mathbf{M} can always be factorized as $\mathbf{M} = \mathbf{U}\mathbf{\Lambda}\mathbf{V}$, where \mathbf{U} and \mathbf{V} are unimodular integer matrices and $\mathbf{\Lambda}$ is a diagonal integer matrix. Furthermore, we can always ensure that the diagonal elements $[\mathbf{\Lambda}]_{ii}$ of $\mathbf{\Lambda}$ are positive integers and $[\mathbf{\Lambda}]_{ii}$ divides $[\mathbf{\Lambda}]_{i+1,i+1}$. In this case, $\mathbf{\Lambda}$ is unique and is called the Smith form of \mathbf{M} .

1.3.2. Basic notions in MD multirate systems

1. *Fourier transform and Z-transform.* Consider a D dimensional signal $x(\mathbf{n})$, where \mathbf{n} is a $D \times 1$ integer column vector. The Fourier transformation and Z-transform of $x(\mathbf{n})$ will be denoted respectively by $X(\mathbf{w})$ and $X(\mathbf{z})$; they will be distinguished by the given argument, \mathbf{w} for Fourier transform and \mathbf{z} for Z-transform. The Fourier transform of $x(\mathbf{n})$ is defined as

$$X(\mathbf{w}) = \sum_{\mathbf{n} \in \mathcal{N}} x(\mathbf{n}) e^{-j\mathbf{w}^T \mathbf{n}},$$

where \mathbf{w} is a $D \times 1$ vector with $\mathbf{w} = (\omega_0 \ \omega_1 \ \dots \ \omega_{D-1})^T$ and \mathcal{N} is the set of all $D \times 1$ integer vectors. The Z-transform of $x(\mathbf{n})$, where it converges, is given by

$$X(\mathbf{z}) = \sum_{\mathbf{n} \in \mathcal{N}} x(\mathbf{n}) \mathbf{z}^{-\mathbf{n}},$$

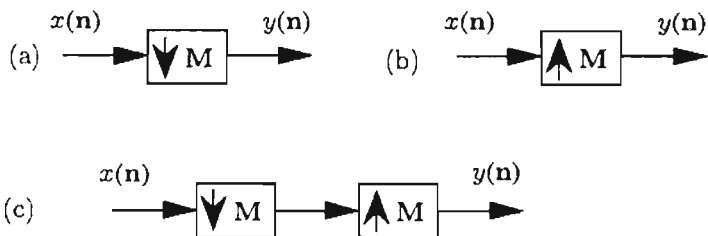


Figure 1.10. (a) The decimation matrix \mathbf{M} , (b) the expansion matrix \mathbf{M} and (c) the decimator followed by expander.

where $\mathbf{z} = (z_0 \ z_1 \ \dots \ z_{D-1})^T$. A vector raised to a vector power, as in $\mathbf{z}^{-\mathbf{n}}$ above, gives a scalar quantity defined as

$$\mathbf{z}^{\mathbf{n}} = z_0^{n_0} z_1^{n_1} \dots z_{D-1}^{n_{D-1}}, \quad \mathbf{n} = (n_0 \ n_1 \ \dots \ n_{D-1})^T.$$

2. A filter $H(\mathbf{z})$ is called Nyquist(\mathbf{M}) if $h(\mathbf{M}\mathbf{n})$ has only one nonzero coefficient. In 1D case, if $M = 2$, $H(z)$ is called a halfband filter.
3. *Decimators and expanders.* For an \mathbf{M} -fold decimator (1.10(a)), the input $x(\mathbf{n})$ and the output $y(\mathbf{n})$ are related by $y(\mathbf{n}) = x(\mathbf{M}\mathbf{n})$. In the frequency domain, the relation is

$$Y(\mathbf{w}) = \frac{1}{J(\mathbf{M})} \sum_{\mathbf{k} \in \mathcal{N}(\mathbf{M}^T)} X(\mathbf{M}^{-T}(\mathbf{w} - 2\pi\mathbf{k})).$$

Given an \mathbf{M} -fold expander (Fig. 1.10(b)), the input $x(\mathbf{n})$ and the output $y(\mathbf{n})$ are related by

$$y(\mathbf{n}) = \begin{cases} x(\mathbf{M}^{-1}\mathbf{n}), & \mathbf{n} \in \text{LAT}(\mathbf{M}) \\ 0, & \text{otherwise.} \end{cases}$$

In the frequency domain, the relation is $Y(\mathbf{w}) = X(\mathbf{M}^T \mathbf{w})$, or equivalently $Y(\mathbf{z}) = X(\mathbf{z}^{\mathbf{M}})$, where $\mathbf{z}^{\mathbf{M}}$ is defined as

$$\mathbf{z}^{\mathbf{M}} = (z^{\mathbf{m}_0} \ z^{\mathbf{m}_1} \ \dots \ z^{\mathbf{m}_{D-1}})^T,$$

with \mathbf{m}_i denoting the i th column of \mathbf{M} .

4. *Decimation followed by expansion.* Consider the concatenation of the \mathbf{M} -fold decimator and the \mathbf{M} -fold expander in Fig. 1.10(c). The input $x(\mathbf{n})$ and the output $y(\mathbf{n})$ are related by

$$y(\mathbf{n}) = \begin{cases} x(\mathbf{n}), & \mathbf{n} \in \text{LAT}(\mathbf{M}) \\ 0, & \text{otherwise.} \end{cases}$$

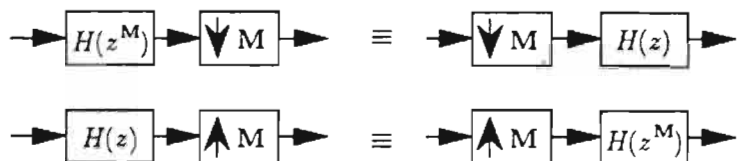


Figure 1.11. Noble identities for multidimensional decimators and expanders.

In the frequency domain, the relation becomes

$$Y(\mathbf{w}) = \frac{1}{J(\mathbf{M})} \sum_{\mathbf{k} \in \mathcal{N}(\mathbf{M}^T)} X(\mathbf{w} - 2\pi \mathbf{M}^{-T} \mathbf{k}).$$

The output $Y(\mathbf{w})$ contains $X(\mathbf{w})$ and $J(\mathbf{M}) - 1$ shifted versions $X(\mathbf{w} - 2\pi \mathbf{M}^{-T} \mathbf{k})$ (images of $X(\mathbf{w})$).

- Noble identities.* Fig. 1.11 shows two useful multirate identities for multidimensional systems. These allow the movement of multirate building blocks across transfer functions under some conditions.
- Perfect reconstruction MD filter bank.* Consider the MD filter bank in Fig. 1.1. Let $\mathcal{N}(\mathbf{M}^T) = \{ \mathbf{k}_i \}_{i=0}^{J(\mathbf{M})-1}$ and the vector $\mathbf{k}_0 = \mathbf{0}$. The output $\hat{X}(\mathbf{w})$ is given by

$$\hat{X}(\mathbf{w}) = T(\mathbf{w})X(\mathbf{w}) + \sum_{i=1}^{J(\mathbf{M})-1} A_i(\mathbf{w})X(\mathbf{w} - 2\pi \mathbf{M}^{-T} \mathbf{k}_i), \quad (1.2)$$

where $T(\mathbf{w})$ is the distortion function and $A_i(\mathbf{w})$ is the i th aliasing transfer function. The distortion function $T(\mathbf{w})$ is defined as

$$T(\mathbf{w}) = \frac{1}{J(\mathbf{M})} \sum_{m=0}^{J(\mathbf{M})-1} H_m(\mathbf{w})F_m(\mathbf{w}).$$

The i th aliasing transfer function $A_i(\mathbf{w})$ is defined as

$$A_i(\mathbf{w}) = \frac{1}{J(\mathbf{M})} \sum_{m=0}^{J(\mathbf{M})-1} H_m(\mathbf{w} - 2\pi \mathbf{M}^{-T} \mathbf{k}_i)F_m(\mathbf{w}).$$

The MD filter bank is free from aliasing if $A_i(\mathbf{w}) = 0$, for $i = 1, 2, \dots, J(\mathbf{M}) - 1$. The filter bank has perfect reconstruction if it is free from aliasing and the distortion function $T(\mathbf{w})$ is a delay. In this case, $\hat{X}(\mathbf{w})$ is a scaled and delayed version of $X(\mathbf{w})$. As in 1D filter banks, the perfect reconstruction condition can be interpreted in terms

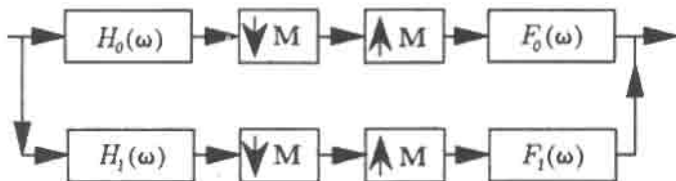


Figure 2.1. Two-dimensional two-channel filter bank, where \mathbf{M} is a 2 by 2 integer matrix with $|\det \mathbf{M}|=2$.

of the polyphase matrices. Using polyphase decomposition, the analysis and synthesis filters have the form

$$H_m(\mathbf{w}) = \sum_{\mathbf{n}_i \in \mathcal{N}(\mathbf{M})} E_{m,i}(\mathbf{M}^T \mathbf{w}) e^{-j\mathbf{w}^T \mathbf{n}_i}, \quad m = 0, 1, \dots, J(\mathbf{M}) - 1,$$

$$F_m(\mathbf{w}) = \sum_{\mathbf{n}_i \in \mathcal{N}(\mathbf{M})} R_{i,m}(\mathbf{M}^T \mathbf{w}) e^{j\mathbf{w}^T \mathbf{n}_i}, \quad m = 0, 1, \dots, J(\mathbf{M}) - 1.$$

The $J(\mathbf{M}) \times J(\mathbf{M})$ matrices $\mathbf{E}(\mathbf{w})$ and $\mathbf{R}(\mathbf{w})$ with $[\mathbf{E}(\mathbf{w})]_{m,i} = E_{m,i}(\mathbf{w})$ and $[\mathbf{R}(\mathbf{w})]_{m,i} = R_{i,m}(\mathbf{w})$ are respectively called the polyphase matrices for the analysis bank and the synthesis bank. The MD filter bank has perfect reconstruction if $\mathbf{R}(\mathbf{w})\mathbf{E}(\mathbf{w}) = \mathbf{I}$.

2. Two-Dimensional Two-Channel Filter Banks

Consider the 2D two-channel filter bank in Fig. 2.1, where the decimation matrix \mathbf{M} is a 2×2 integer matrix with $|\det \mathbf{M}| = 2$. For the diamond filter bank, the decimation matrix is usually the quincunx matrix \mathbf{Q} as defined in (1.1). The supports of the analysis filters are shown in Fig. 1.4. As there are only four filters in the filter bank, two analysis and two synthesis filters, it is possible to design perfect reconstruction diamond filter bank without direct optimization of 2D filters. The design can be first reduced to that of two 2D filters, which can be further reduced to the design of 1D filters. More precisely, we can design the diamond filter bank by the following two steps.

1. *Reducing the design of the diamond filter bank to that of two 2D filters* [1]. If we choose $H_1(\mathbf{z})$ and $F_1(\mathbf{z})$ appropriately, we can reduce the design of the diamond filter bank to that of $H_0(\mathbf{z})$ and $F_0(\mathbf{z})$. In this case, the filter bank has perfect reconstruction if and only if $H_0(\mathbf{z})F_0(\mathbf{z})$ is Nyquist(\mathbf{Q}). (The definition of a Nyquist(\mathbf{Q}) filter is as given in Sec. 1.3.2.) So the design of the diamond filter bank is reduced to the design of 2D filters $H_0(\mathbf{z})$ and $F_0(\mathbf{z})$.
2. *Design of $H_0(\mathbf{z})$ and $F_0(\mathbf{z})$ such that $H_0(\mathbf{z})F_0(\mathbf{z})$ is Nyquist(\mathbf{M})*. Two approaches can be used to carry out this step. Both design techniques involve only the design of 1D filters; no 2D optimization is required. In the first approach [1], the McClellan transformation is employed to convert the 2D filter design problem to a similar 1D problem. In the second approach [24], [38], we will use a Nyquist(\mathbf{M}) approach to further simplify the

design of $H_0(\mathbf{z})$ and $F_0(\mathbf{z})$ to the design of a Nyquist(\mathbf{Q}) filter $H_0(\mathbf{z})$ only. After this, we use the so-called polyphase mapping [24], [38] to design the 2D filter $H_0(\mathbf{z})$ from a 1D filter.

We will see that the above design procedures can be applied to the quadrant filter bank (Fig. 1.5) with some modifications.

2.1. Design of the Diamond Filter Bank

2.1.1. Reducing the filter bank design problem to a constrained 2D filter-design problem

Consider the filter bank in Fig. 2.1 with decimation matrix $\mathbf{M} = \mathbf{Q}$, where \mathbf{Q} is as defined in (1.1). With this choice of \mathbf{M} , it can be verified from (1.2) that the output $\hat{X}(\mathbf{z})$ and input $X(\mathbf{z})$ are related by $\hat{X}(\mathbf{z}) = A(\mathbf{z})X(-\mathbf{z}) + T(\mathbf{z})X(\mathbf{z})$, where $A(\mathbf{z})$ and $T(\mathbf{z})$ are respectively the alias transfer function and the distortion function given by

$$\begin{aligned} A(\mathbf{z}) &= \frac{1}{2} (H_0(-\mathbf{z})F_0(\mathbf{z}) + H_1(-\mathbf{z})F_1(\mathbf{z})) \\ T(\mathbf{z}) &= \frac{1}{2} (H_0(\mathbf{z})F_0(\mathbf{z}) + H_1(\mathbf{z})F_1(\mathbf{z})). \end{aligned} \quad (2.1)$$

The system is alias free if the alias transfer function $A(\mathbf{z}) = 0$. The system has perfect reconstruction if it is alias free and the distortion function $T(\mathbf{z})$ is a delay. For alias cancellation, we choose the following highpass analysis and synthesis filters

$$H_1(\mathbf{z}) = z_0^{-1} F_0(-\mathbf{z}), \quad F_1(\mathbf{z}) = z_0 H_0(-\mathbf{z}). \quad (2.2)$$

With this choice, the alias cancellation condition $A(\mathbf{z}) = 0$ is satisfied. Furthermore, $H_1(\mathbf{z})$ and $F_1(\mathbf{z})$ will have the desired support if $H_0(\mathbf{z})$ and $F_0(\mathbf{z})$ have the desired support of the lowpass filters in Fig. 1.4. In this case the distortion function is

$$T(\mathbf{z}) = \frac{1}{2} (H_0(\mathbf{z})F_0(\mathbf{z}) + H_0(-\mathbf{z})F_0(-\mathbf{z})),$$

which is a delay if and only if $H_0(\mathbf{z})F_0(\mathbf{z})$ is a Nyquist(\mathbf{Q}) filter.

So the design of perfect reconstruction diamond filter bank reduces to the design of diamond-shaped $H_0(\mathbf{z})$ and $F_0(\mathbf{z})$ such that $H_0(\mathbf{z})F_0(\mathbf{z})$ is a Nyquist(\mathbf{Q}) filter.

2.1.2. Design of $H_0(\mathbf{z})$ and $F_0(\mathbf{z})$ such that $H_0(\mathbf{z})F_0(\mathbf{z})$ is Nyquist(\mathbf{Q}): method 1

In method 1, we will use the McClellan transformation to simplify the design problem of 2D filters $H_0(\mathbf{z})$ and $F_0(\mathbf{z})$. In particular, we can convert the design of $H_0(\mathbf{z})$ and $F_0(\mathbf{z})$ into a similar 1D problem: design of 1D filters $H(z)$ and $F(z)$ such that $H(z)F(z)$ is halfband (i.e., Nyquist(2)). The analysis and synthesis filters in this case are FIR and linear-phase.

McClellan transformation. This transformation was proposed by McClellan in 1976 and has been since a popular method in designing 2D filters [15], [36]. It converts a

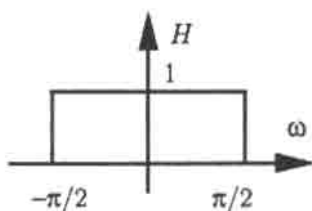


Figure 2.2. The desired response of $H(\omega)$.

1D zero phase filter into a 2D zero phase filter. The procedure of applying McClellan transformation on a 1D zero phase filter $P(z)$ is as follows. Any 1D zero phase filter $P(z)$ with real coefficients can be expressed in the form $P(z) = \sum_{n=0}^K \hat{p}(n)(z + z^{-1})^n$, where $\hat{p}(n)$ is real. Thus $P(z) = \hat{P}(z + z^{-1})$, where $\hat{P}(x)$ is the polynomial $\hat{P}(x) = \sum_{n=0}^K \hat{p}(n)x^n$. Given such a 1D filter $P(z)$, consider the 2D filter defined from the underlying polynomial $\hat{P}(x)$ as follows

$$\begin{aligned}
 P_0(z_0, z_1) &= \hat{P}(M(z_0, z_1)), \quad \text{where} \\
 M(z_0, z_1) &= a_0 + a_1(z_0 + z_0^{-1}) + a_2(z_1 + z_1^{-1}) \\
 &\quad + a_3(z_0 z_1^{-1} + z_0^{-1} z_1) + a_4(z_0 z_1 + z_0^{-1} z_1^{-1}).
 \end{aligned} \tag{2.3}$$

With different choice of a_i , the 2D filter $P_0(z)$ has different frequency response.

For our purpose, the appropriate choice of $M(z_0, z_1)$ is $M_d(z_0, z_1)$, where

$$M_d(z_0, z_1) = \frac{1}{2}(z_0 + z_0^{-1} + z_1 + z_1^{-1}). \tag{2.4}$$

If the 1D filter $P(z)$ is lowpass as shown in Fig. 2.2, then $P_0(z)$ has a diamond-shaped support as shown in Fig. 1.4(a). Furthermore, it can be verified that if the 1D filter $P(z)$ is half-band, then the 2D filter $P_0(z)$ is Nyquist(Q).

The two steps involved in designing the analysis bank $\{H_0(z), F_0(z)\}$ are:

1. Design 1D zero-phase filters $H(z)$ and $F(z)$ such that $D(z) = H(z)F(z)$ is halfband.
2. Apply the McClellan transformation $M_d(z)$ on $H(z)$ and $F(z)$ to get the 2D filters $H_0(z)$ and $F_0(z)$.

If the 1D filters $H(z)$ and $F(z)$ are lowpass as in Fig. 2.2, the 2D filters $H_0(z)$ and $F_0(z)$ have the desired diamond support shown in Fig. 1.4(a). As $H(z)F(z)$ is halfband, the product filter $H_0(z)F_0(z)$ is Nyquist(Q); perfect reconstruction is guaranteed. Because the 2D filters designed through the McClellan transformation are FIR and linear-phase, all the analysis and synthesis filters are FIR and linear-phase. We observe that the remaining nontrivial part of this technique is the design of 1D zero-phase filters $H(z)$ and $F(z)$ such that $H(z)F(z)$ is halfband. The design of such $H(z)$ and $F(z)$ is discussed next.

We will discuss two approaches for this. These two approaches are elaborated below.

1. Factorization approach [1]. We can first design a zero-phase halfband $D(z)$ and then factorize $D(z)$ into linear phase $H(z)$ and $F(z)$. The technique described in [47] can be used to design linear-phase halfband $D(z)$. We can also choose $D(z)$ to be a Lagrange filter [45], which is a well-known class of zero-phase halfband filters that can be expressed in closed form. However, this design of $H(z)$ and $F(z)$ involves factorization of $D(z)$. We will see that the Nyquist(2) approach to be introduced next requires no factorization.

2. Nyquist(2) approach [25], [38]. Suppose $H(z)$ itself is a Nyquist(2) (i.e., halfband) filter. It can be verified if $H(z)F(z)$ has to be halfband, then $F(z)$ is necessarily of the form $F(z) = 1 + (2\gamma(z) - 1)H(-z)$, for some halfband filter $\gamma(z)$. Conversely, $H(z)F(z)$ is a halfband filter for any choice of halfband $H(z)$ and $\gamma(z)$. For simplicity, let us choose $\gamma(z) = H(z)$. Then

$$F(z) = 1 + (2H(z) - 1)H(-z).$$

It follows that if $H(z)$ is lowpass, $F(z)$ is also lowpass. Zero-phase property of $H(z)$ implies zero-phase property of $F(z)$. Through this approach, we only need to design $H(z)$, which can be easily done using any design technique for linear phase halfband filters. This Nyquist(2) approach can be extended to 2D case and the 2D extension will be the first step for the second design method of $H_0(z)$ and $F_0(z)$.

2.1.3. Design of $H_0(z)$ and $F_0(z)$ such that $H_0(z)F_0(z)$ is Nyquist(Q): method 2

This method can be described by the following two steps, [24], [38].

Step 1. Use a Nyquist(Q) approach to simplify the design of $H_0(z)$ and $F_0(z)$ to only the design of a Nyquist(Q) filter $H_0(z)$. Step 2. Design a Nyquist(Q) filter $H_0(z)$ with a diamond support.

The resulting filter bank has some very attractive properties. The individual filters can be FIR or IIR. Detailed discussion will be given in Sec. 2.3.

Step 1. Nyquist(Q) approach. Let $H_0(z)$ be a Nyquist(Q) filter and $H_0(z) + H_0(-z) = 1$. We can verify that if $H_0(z)F_0(z)$ is also Nyquist(Q), then $F_0(z)$ is necessarily of the form $F_0(z) = 1 + (2\gamma(z) - 1)H_0(-z)$, for some Nyquist(Q) filter $\gamma(z)$. For simplicity, we can choose $\gamma(z) = H_0(z)$, then

$$F_0(z) = 1 + (2H_0(z) - 1)H_0(-z).$$

For this choice of $F_0(z)$, the product filter $H_0(z)F_0(z)$ is Nyquist(Q) if $H_0(z)$ is Nyquist(Q). So perfect reconstruction of the diamond filter bank is guaranteed if $H_0(z)$ is Nyquist(Q). As Nyquist(Q) is the only condition on $H_0(z)$, $H_0(z)$ can be FIR or IIR. Furthermore, if $H_0(z)$ has a diamond-shaped support as shown in Fig. 1.4(a), $F_0(z)$ has the same diamond-shaped support. So the remaining task is to design $H_0(z)$ such that it is Nyquist(Q) and has the diamond support in Fig. 1.4(a).

Step 2. Design of Nyquist(Q) $H_0(z)$ with a diamond support. The McClellan transformation can be used to design such $H_0(z)$. Let $H(z)$ be a 1D zero-phase halfband filter with support as shown in Fig. 2.2. By using the McClellan transformation in (2.4) on $H(z)$, we can obtain a Nyquist(Q) filter $H_0(z)$ with a diamond support. Because the 2D filters designed through McClellan transformation are FIR and have linear phase, all the analysis and synthesis filters are FIR and are constrained to have linear phase. Next, we use a polyphase mapping method to design $H_0(z)$. In this method, $H_0(z)$ can be FIR or IIR and need not have linear phase in FIR case.

Polyphase mapping approach. As $H_0(z)$ is Nyquist(Q), without loss of generality, it can be expressed as

$$H_0(z) = \frac{1}{2}(1 + z_0^{-1}\beta(z^Q)).$$

In this case, $H_0(z)$ remains Nyquist(Q) for any choice of $\beta(z)$. Also let $H(z)$ be a 1D halfband filter with support as shown in Fig. 2.2, then $H(z)$ can be expressed as

$$H(z) = \frac{1}{2}(1 + z^{-1}\alpha(z^2)). \quad (2.5)$$

We will see that if we choose

$$\beta(z) = \alpha(z_0)\alpha(z_1), \quad (2.6)$$

then $H_0(z)$ has the desired diamond support. The 1D polyphase component $\alpha(z)$ can be FIR or IIR and hence the 2D filter $H_0(z)$ can be FIR or IIR. As $\alpha(z)$ is the polyphase component of the 1D filter $H(z)$ and $\beta(z)$ is the polyphase component of the 2D filter $H_0(z)$, this method is termed the polyphase mapping method. This mapping can also be obtained by starting from the transformation reported in [9].

The reason why the mapping in (2.6) gives the desired response for $H_0(z)$ is as follows. Notice that if $H(z)$ is lowpass with support as shown in Fig. 2.2, then

$$z^{-1}\alpha(z^2) \approx \begin{cases} 1, & \omega \in (-\pi/2, \pi/2) \\ -1, & \text{otherwise.} \end{cases} \quad (\text{see Fig. 2.3}) \quad (2.7)$$

It follows that

$$(z_0z_1)^{-1/2}\alpha(z_0z_1) \approx \begin{cases} 1, & (\omega_0 + \omega_1) \in (-\pi, \pi), \\ -1, & \text{otherwise,} \end{cases} \quad (\text{see Fig. 2.4(a)})$$

$$\text{and } (z_0z_1^{-1})^{-1/2}\alpha(z_0z_1^{-1}) \approx \begin{cases} 1, & (\omega_0 - \omega_1) \in (-\pi, \pi), \\ -1, & \text{otherwise.} \end{cases} \quad (\text{see Fig. 2.4(b)})$$

So $z_0^{-1}\beta(z^Q) = z_0^{-1}\alpha(z_0z_1)\alpha(z_0z_1^{-1})$, which is the product of $(z_0z_1)^{-1/2}\alpha(z_0z_1)$ and $(z_0z_1^{-1})^{-1/2}\alpha(z_0z_1^{-1})$, has the following response

$$z_0^{-1}\beta_0(z^Q) \approx \begin{cases} 1, & \mathbf{w} \text{ in the diamond region in Fig. 1.4(a).} \\ -1, & \text{otherwise.} \end{cases} \quad (\text{see Fig. 2.4(c)})$$

Fig. 2.4(c) implies that $H_0(\mathbf{w})$ has the desired diamond support.

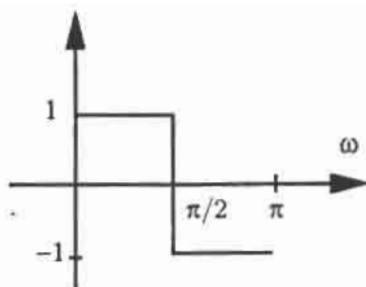


Figure 2.3. The ideal response of $z^{-1}\alpha(z^2)$.

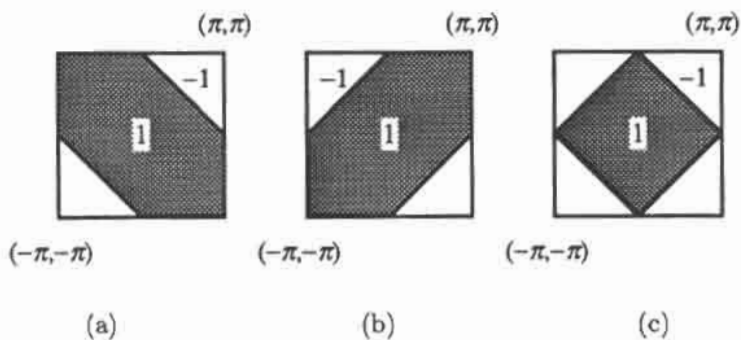


Figure 2.4. The ideal responses of (a) $(z_0 z_1)^{-1/2} \alpha(z_0 z_1)$, (b) $(z_0 z_1^{-1})^{-1/2} \alpha(z_0 z_1^{-1})$, and (c) $z_0^{-1} \beta(\mathbf{x}^Q)$ for the diamond filter bank.

2.2. Design of the Quadrant Filter Bank

2.2.1. Reducing the filter bank design to a constrained 2D filter-design problem

For the quadrant filter bank, the decimation matrix will be denoted as \mathbf{D} , where

$$\mathbf{D} = \begin{pmatrix} 2 & 0 \\ 0 & 1 \end{pmatrix}. \quad (2.8)$$

Consider the filter bank in Fig. 2.1 with decimation matrix $\mathbf{M} = \mathbf{D}$. The output $\widehat{X}(\mathbf{z})$ and input $X(\mathbf{z})$ in this case are related by $\widehat{X}(\mathbf{z}) = A(\mathbf{z})X(-z_0, z_1) + T(\mathbf{z})X(\mathbf{z})$. The alias transfer function $A(\mathbf{z})$ is given by

$$A(\mathbf{z}) = \frac{1}{2} (H_0(-z_0, z_1)F_0(\mathbf{z}) + H_1(-z_0, z_1)F_1(\mathbf{z})).$$

The distortion function $T(\mathbf{z})$ is as given in (2.1). Consider the following choice of the filters $H_1(\mathbf{z})$ and $F_1(\mathbf{z})$.

$$H_1(\mathbf{z}) = z_0^{-1}F_0(-z_0, z_1), \quad F_1(\mathbf{z}) = z_0H_0(-z_0, z_1).$$

This choice gives us exact cancellation of aliasing, i.e. $A(\mathbf{z}) = 0$. Also $H_1(\mathbf{z})$ and $F_1(\mathbf{z})$ have the desired support as in Fig. 1.5(b) if $H_0(\mathbf{z})$ and $F_0(\mathbf{z})$ have supports in quadrant I and III as in Fig. 1.5(a). For the above choice of filters, the distortion function is given by

$$T(\mathbf{z}) = \frac{1}{2} (H_0(\mathbf{z})F_0(\mathbf{z}) + H_0(-z_0, z_1)F_0(-z_0, z_1)).$$

The quadrant filter bank has perfect reconstruction if and only if $H_0(\mathbf{z})F_0(\mathbf{z})$ is Nyquist(\mathbf{D}). Similar to the diamond case, the design problem of the filter bank reduces to the design of quadrant filters $H_0(\mathbf{z})$ and $F_0(\mathbf{z})$ such that $H_0(\mathbf{z})F_0(\mathbf{z})$ is a Nyquist(\mathbf{D}) filter.

2.2.2. Design of $H_0(z)$ and $F_0(z)$ such that $H_0(z)F_0(z)$ is Nyquist(\mathbf{D}): method 1

In the diamond filter bank, we have used a special case of McClellan transformation, namely (2.4), to design a 2D diamond-shaped filter. Here we will consider a different choice of McClellan transformation that converts a 1D zero-phase lowpass filter into a 2D quadrant filter. Let $P(z)$ be a 1D zero-phase filter with support as in Fig. 2.2. Consider the McClellan transformation

$$M_q(\mathbf{z}) = \frac{1}{2} (z_0z_1 + z_0^{-1}z_1^{-1} - z_0z_1^{-1} - z_0^{-1}z_1). \quad (2.9)$$

If we apply this transformation on $P(z)$, the resulting 2D filter $P_0(\mathbf{z})$ has quadrant support as shown in Fig. 1.5(a). Moreover, if the 1D filter $P(z)$ is halfband, then $P_0(\mathbf{z})$ is Nyquist(\mathbf{D}).

As in the diamond case, let $H(z)$ and $F(z)$ have support as in Fig. 2.2 and let $H(z)F(z)$ be a halfband filter. Then we apply the McClellan transformation described in (2.9) on

$H(z)$ and $F(z)$ to obtain 2D filters $H_0(\mathbf{z})$ and $F_0(\mathbf{z})$. The resulting $H_0(\mathbf{z})$ and $F_0(\mathbf{z})$ are quadrant filters as in Fig. 1.5(a). As $H(z)F(z)$ is halfband, $H_0(\mathbf{z})F_0(\mathbf{z})$ is a Nyquist(**D**) filter; perfect reconstruction of the quadrant filter bank is assured. Also, as the 2D filters designed through the McClellan transformation are FIR and linear-phase, all the analysis and synthesis filters are FIR and linear-phase.

2.2.3. Design of $H_0(\mathbf{z})$ and $F_0(\mathbf{z})$ such that $H_0(\mathbf{z})F_0(\mathbf{z})$ is Nyquist(**D**): method 2

This technique is very similar to the one proposed for the diamond filter bank in Sec. 2.1.3. In this design, the individual filters can be FIR or IIR. This method can be described by the following two steps. Step 1. Use a Nyquist(**D**) approach to simplify the design of $H_0(\mathbf{z})$ and $F_0(\mathbf{z})$ to only the design of a Nyquist(**D**) filter $H_0(\mathbf{z})$. Step 2. Design a Nyquist(**D**) filter $H_0(\mathbf{z})$ with the quadrant support in Fig. 1.5(a).

Step 1. Nyquist(D**) approach.** Let $H_0(\mathbf{z})$ be a Nyquist(**D**) filter and $H_0(\mathbf{z}) + H_0(-z_0, z_1) = 1$. We can verify that if $H_0(\mathbf{z})F_0(\mathbf{z})$ is Nyquist(**D**), then $F_0(\mathbf{z})$ is of the form $F_0(\mathbf{z}) = 1 + (2\gamma(\mathbf{z}) - 1)H_0(-z_0, z_1)$, for some Nyquist(**D**) filter $\gamma(\mathbf{z})$. For simplicity, let us choose $\gamma(\mathbf{z}) = H_0(\mathbf{z})$, then

$$F_0(\mathbf{z}) = 1 + (2H_0(\mathbf{z}) - 1)H_0(-z_0, z_1).$$

For this choice of $F_0(\mathbf{z})$, the product filter $H_0(\mathbf{z})F_0(\mathbf{z})$ remains Nyquist(**D**) for any Nyquist(**D**) filter $H_0(\mathbf{z})$. So perfect reconstruction of the quadrant filter bank is guaranteed if $H_0(\mathbf{z})$ is Nyquist(**Q**). The only condition on $H_0(\mathbf{z})$ is that $H_0(\mathbf{z})$ should be Nyquist(**D**); $H_0(\mathbf{z})$ can be FIR or IIR. Furthermore, if $H_0(\mathbf{z})$ has a quadrant support as shown in Fig. 1.5(a), then $F_0(\mathbf{z})$ has the same quadrant support. The remaining task is to design the Nyquist(**D**) filter $H_0(\mathbf{z})$ with support as in Fig. 1.5(a).

Step 2. Design of Nyquist(D**) $H_0(\mathbf{z})$.** Similar to the design of filter bank with diamond filters, the McClellan transformation can be used to design $H_0(\mathbf{z})$. Let the 1D filter $H(z)$ be linear-phase and has support as in Fig. 2.2. By using the McClellan transformation in (2.9) on $H(z)$, we can obtain a Nyquist(**D**) filter $H_0(\mathbf{z})$ with a quadrant support as in (Fig. 1.5(a)). In this case, all the analysis and synthesis filters are FIR and are constrained to have linear phase. Next we design $H_0(\mathbf{z})$ using a polyphase mapping method, which is similar to the one introduced for the diamond filter in (2.6). In this method, $H_0(\mathbf{z})$ can be FIR or IIR and need not have linear phase in FIR case.

Polyphase mapping. As $H_0(\mathbf{z})$ is Nyquist(**D**), without loss of generality, $H_0(\mathbf{z})$ assumes the form

$$H_0(\mathbf{z}) = \frac{1}{2}(1 + z_0^{-1}\beta(\mathbf{z}^{\mathbf{D}})).$$

Let $H(z)$ be a 1D halfband filter as (2.5) and the support of $H(z)$ be as shown in Fig. 2.2. We will see that if we choose

$$\beta(\mathbf{z}) = -z_1^{-1}\alpha(-z_0)\alpha(-z_1^2), \quad (2.10)$$

then $H_0(\mathbf{z})$ has the desired quadrant support. This polyphase mapping is similar to the one proposed in (2.6) for diamond filters. In this case, the 1D polyphase component $\alpha(z)$ can

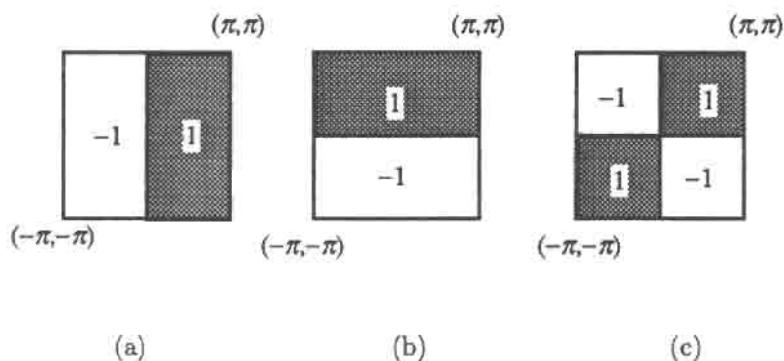


Figure 2.5. The ideal responses of (a) $jz_0\alpha(-z_0^2)$, (b) $jz_1\alpha(-z_1^2)$, and (c) $z_0^{-1}\beta(\mathbf{z}^{\mathbf{D}})$ for the quadrant filter bank.

also be FIR or IIR and hence the 2D filter $H_0(\mathbf{z})$ can be FIR or IIR. The reason why the mapping in (2.10) gives the desired response is given next.

From (2.7), we have

$$(jz_0)\alpha(-z_0^2) \approx \begin{cases} 1, & \omega_0 \in (0, \pi), \\ -1, & \text{otherwise,} \end{cases} \quad (\text{see Fig. 2.5(a)})$$

$$(jz_1)\alpha(-z_1^2) \approx \begin{cases} 1, & \omega_1 \in (0, \pi), \\ -1, & \text{otherwise,} \end{cases} \quad (\text{see Fig. 2.5(b)})$$

Therefore, $z_0^{-1}\beta(\mathbf{z}^{\mathbf{D}}) = -z_0^{-1}z_1^{-1}\alpha(-z_0^2)\alpha(-z_1^2)$ has the following response

$$z_0^{-1}\beta_0(\mathbf{z}^{\mathbf{D}}) \approx \begin{cases} 1, & \mathbf{w} \in \text{quadrants I and III,} \\ -1, & \text{otherwise.} \end{cases} \quad (\text{see Fig. 2.5(c)})$$

Fig. 2.5(c) implies that $H_0(\mathbf{z})$ has the desired support.

2.3. Properties due to the second design technique of $H_0(\mathbf{z})$ and $F_0(\mathbf{z})$

For both the diamond and the quadrant filter banks, we have described two techniques to design $H_0(\mathbf{z})$ and $F_0(\mathbf{z})$ such that $H_0(\mathbf{z})F_0(\mathbf{z})$ is Nyquist(M). When the second design technique (Sec. 2.1.3 for the diamond filter bank and Sec. 2.2.3 for the quadrant filter bank) is used, the filter bank has some very attractive properties.

Robust ladder structure. When Nyquist(M) approach is used to design $H_0(\mathbf{z})$ and $F_0(\mathbf{z})$, the proposed filter bank has a very attractive ladder structure implementation (Fig. 2.6), which is robust to roundoff noise [38]. For the diamond filter bank, $\beta(\mathbf{z})$ is as in (2.6), and $\mathbf{d} = (1 \ 1)^T$. For the quadrant filter bank, $\beta(\mathbf{z})$ is as in (2.10), and $\mathbf{d} = (1 \ 0)^T$. Perfect reconstruction is preserved even when coefficients of $\beta(\mathbf{z})$ are quantized.

If we further use the polyphase mapping method to design the Nyquist(M) filter $H_0(\mathbf{z})$, the filter bank has the following additional three properties.

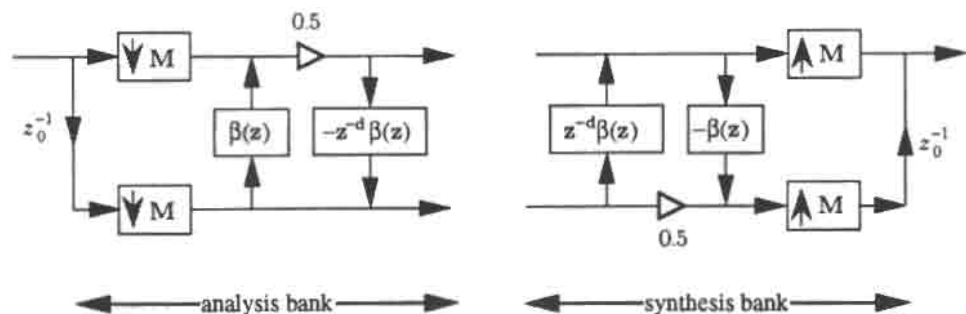


Figure 2.6. The implementation of the diamond filter bank or the quadrant filter bank that is designed through the Nyquist(M) approach.

1. *Stability and causality in IIR case.* Because the the 1D filter $H(z)$ in (2.5) can be FIR or IIR, its polyphase component $\alpha(z)$ can be FIR or IIR. So the 2D analysis filters can be FIR or IIR. In the IIR case, it is shown in [38] that the 2D analysis and synthesis filters will always be causal and stable if $\alpha(z)$ is causal and stable. Also in the IIR case, $\alpha(z)$ can be taken to be an allpass function. The allpass functions can be implemented through a low-sensitivity lattice structure [50], which guarantees stability in spite of multiplier quantization.
2. *Linear-phase in FIR case.* If the 1D filter $\alpha(z)$ is a Type 2 linear-phase filter [50], the analysis and synthesis filters have linear phase.
3. *Complexity.* From the implementation in Fig. 2.6, we observe that the complexity of the analysis bank is comparable to that of $\beta(z)$ (due to the fact that all the operations are at a lower rate). For both diamond and quadrant filter banks, $\beta(z)$ is a separable filter and the cost of $\beta(z)$ is equivalent to twice that of the 1D filter $\alpha(z)$.

Example 2.1. FIR diamond filter bank. In this example, we use the technique described in Sec. 2.1.3 to design $H_0(z)$ and $F_0(z)$. We first design 1D FIR halfband filter $H(z)$ that has zero phase and has support as in Fig. 2.2. Then we use the polyphase mapping method to obtain the 2D Nyquist(Q) filter $H_0(z)$ from $H(z)$. As $H_0(z)$ is Nyquist(Q), the diamond filter bank has perfect reconstruction. Due to the polyphase mapping method, $H_0(z)$ is FIR and linear-phase and hence all the analysis and synthesis filters are FIR and linear-phase. Fig. 2.7(a) and Fig. 2.7(b) show respectively the magnitude responses of $H_0(z)$ and $H_1(z)$. The stopband attenuation $\delta(H_0) \approx 40$ dB and $\delta(H_1) \approx 30$ dB. From (2.2), we observe that the magnitude response of the synthesis filters are shifted version of the analysis filters and hence are not shown.

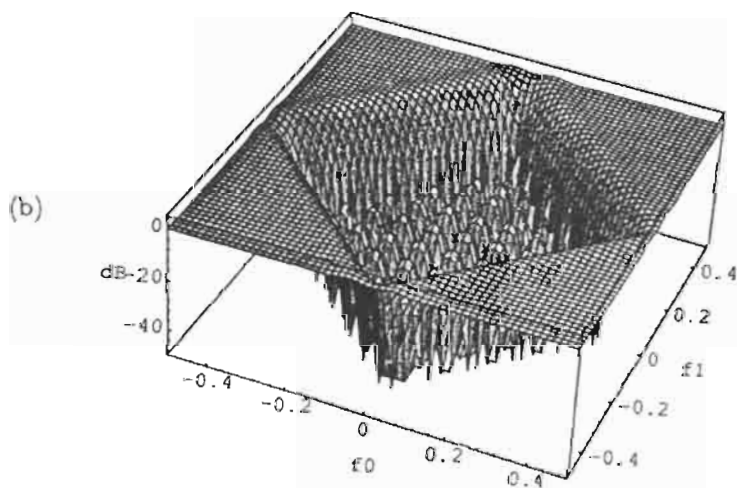
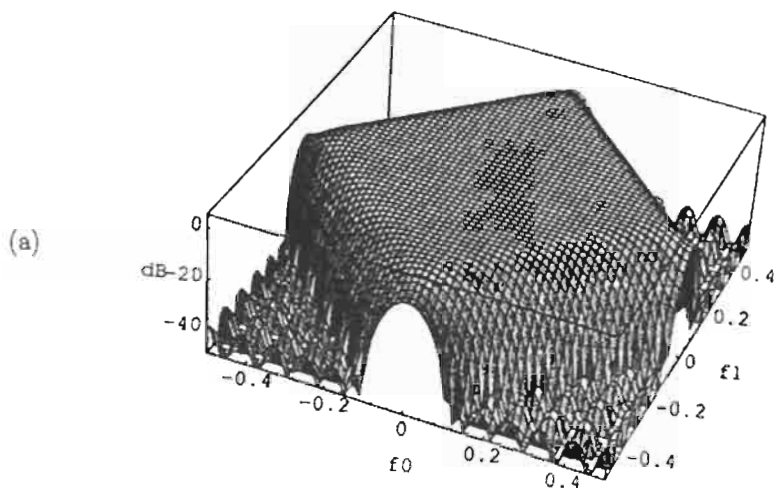


Figure 2.7. Example 2.1. The FIR diamond filter bank. (a) The magnitude response (dB) of $H_0(z)$ and (b) the magnitude response (dB) of $H_1(z)$.

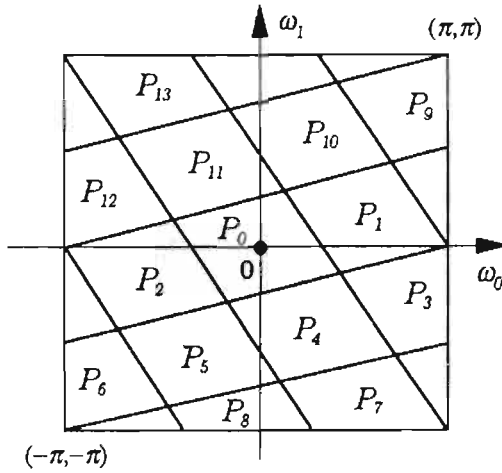


Figure 3.1. DFT filter bank with decimation matrix \mathbf{N} .

3. Designs of MD Multiple Channel Filter Banks Using Transformations

3.1. Uniform DFT Filter Bank

One-dimensional uniform DFT filter banks are described in [12], [50]. In these systems, a set of M filters are derived from a prototype $P(z)$ by using the DFT matrix. The prototype $P(z)$ has bandwidth $2\pi/M$ and all the filters are uniformly shifted versions of $P(z)$. The shifted amounts are $2\pi k/M$, for $k = 1, 2, \dots, M - 1$. Extending the DFT filter bank to the MD case with decimation matrix \mathbf{M} , the prototype $P(z)$ has support $SPD(\pi\mathbf{M}^{-T})$ and other filters in the filter bank are shifts of $P(z)$ by $2\pi\mathbf{M}^{-T}\mathbf{m}$, $\mathbf{m} \in \mathcal{N}(\mathbf{M}^T)$, where $SPD(\cdot)$ and $\mathcal{N}(\cdot)$ are as defined in Sec. 1.3.1. For example, let $\mathbf{M} = \begin{pmatrix} 3 & -1 \\ 2 & 4 \end{pmatrix}$. This has $|\det \mathbf{M}| = 14$ and the supports of the fourteen filters are as depicted in Fig. 3.1. Expressing $P(z)$ in terms of the polyphase components (defined in Sec. 1.3.2), we have

$$P(\mathbf{w}) = \sum_{i=0}^{J(\mathbf{M})-1} E_i(\mathbf{M}^T \mathbf{w}) e^{-j\mathbf{w}^T \mathbf{n}_i}, \quad \mathbf{n}_i \in \mathcal{N}(\mathbf{M}), \quad (3.1)$$

where $E_i(\mathbf{w})$ are the polyphase components of $P(z)$ and $J(\mathbf{M}) = |\det \mathbf{M}|$. Then the MD DFT filter bank can be implemented as in Fig. 3.2. The $J(\mathbf{M}) \times J(\mathbf{M})$ matrix $\mathbf{W}^{(g)}$ is called the generalized DFT matrix with elements given by

$$[\mathbf{W}^{(g)}]_{in} = e^{-j2\pi \mathbf{k}_i^T \mathbf{M}^{-1} \mathbf{m}_n}, \quad \mathbf{m}_n \in \mathcal{N}(\mathbf{M}), \quad \mathbf{k}_i \in \mathcal{N}(\mathbf{M}^T).$$

As \mathbf{M} is an integer matrix, it admits the decomposition $\mathbf{M} = \mathbf{U}\mathbf{A}\mathbf{V}$, where \mathbf{U} and \mathbf{V} are unimodular and \mathbf{A} is a diagonal matrix with $[\mathbf{A}]_{ii} = \lambda_i$ (see Sec. 1.3.1 for a review of diagonalization of integer matrices). It can be shown that $\mathbf{W}^{(g)}$ assumes the form

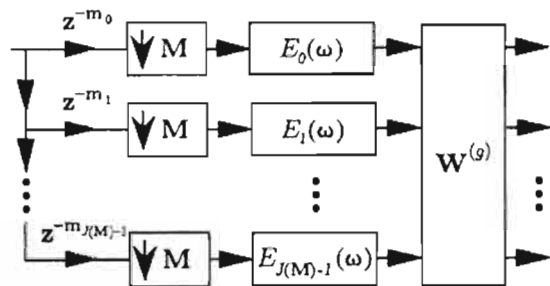


Figure 3.2. The implementation of the MD DFT filter bank, where $\mathbf{W}^{(g)}$ is the generalized DFT matrix.

$$\mathbf{W}^{(g)} = \mathbf{Q}_1 (\mathbf{W}_{\lambda_0} \otimes \mathbf{W}_{\lambda_1} \otimes \dots \otimes \mathbf{W}_{\lambda_{D-1}}) \mathbf{Q}_2,$$

where \mathbf{Q}_1 and \mathbf{Q}_2 are permutation matrices, and \otimes denotes the Kronecker product. The Kronecker product of two matrices \mathbf{A} and \mathbf{B} is defined as

$$\underbrace{\mathbf{A}}_{I \times K} \otimes \underbrace{\mathbf{B}}_{J \times L} = \underbrace{\begin{pmatrix} a_{0,0}\mathbf{B} & \dots & a_{0,K-1}\mathbf{B} \\ \vdots & \dots & \vdots \\ a_{I-1,0}\mathbf{B} & \dots & a_{I-1,K-1}\mathbf{B} \end{pmatrix}}_{IJ \times KL}.$$

When \mathbf{m}_i and \mathbf{k}_j are properly ordered, \mathbf{Q}_1 and \mathbf{Q}_2 become identity matrices. More specifically, suppose we define these sets of vectors to be

$$\mathbf{m}_n = \mathbf{U}\mathbf{n} \bmod \mathbf{M}, \quad \mathbf{k}_n = \mathbf{V}^T \mathbf{n} \bmod \mathbf{M}^T, \quad \mathbf{n} = (n_0 \ n_1 \ \dots \ n_{D-1})^T,$$

with subscripts n computed as follows

$$n = n_0 + \lambda_0 n_1 + (\lambda_0 \lambda_1) n_2 + \dots + (\lambda_0 \lambda_1 \dots \lambda_{D-2}) n_{D-1}. \quad (3.2)$$

Then we will have $\mathbf{Q}_1 = \mathbf{Q}_2 = \mathbf{I}$. Next, we discuss how to design filters with support $SPD(\mathbf{M}^{-T})$. The method to be introduced below has great design efficiency.

MD filter derived from 1D filter [9]. Recall for a 1D N -fold decimator, the output $Y(\omega)$ is a stretched version of the input $X(\omega)$ by N . For example, consider an input $X(\omega)$ with support $SPD(\pi S)$ (Fig. 3.3(a)). Then the output $Y(\omega)$ will have support $SPD(\pi NS)$ as in (3.3)(b) (assuming no aliasing). Similar situation takes place for MD decimators: the output of an decimation matrix \mathbf{N} is the input "stretched by \mathbf{N}^T ". That is if the input has support $SPD(\pi S)$ for some matrix \mathbf{S} , then the output has support $SPD(\pi \mathbf{N}^T \mathbf{S})$ (assuming no aliasing). We will use this property to design MD filters.

Consider the adjugate of \mathbf{M} defined as $\widehat{\mathbf{M}} \triangleq J(\mathbf{M})\mathbf{M}^{-1}$. By definition, $\widehat{\mathbf{M}}$ is also an integer matrix. We will see that if the input $X(\mathbf{w})$ of an $\widehat{\mathbf{M}}$ -fold decimator has support $SPD(\frac{\pi}{J(\widehat{\mathbf{M}})} \mathbf{I})$, then the output $Y(\mathbf{w})$ has support $SPD(\pi \mathbf{M}^{-T})$. The reason is as follows. Due to $\widehat{\mathbf{M}}$ -fold

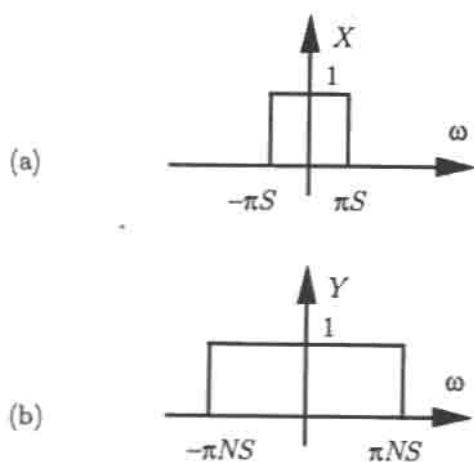


Figure 3.3. Relation of the input support and the output support for an N -fold decimator. The output $Y(\omega)$ is a stretched version of the input $X(\omega)$.

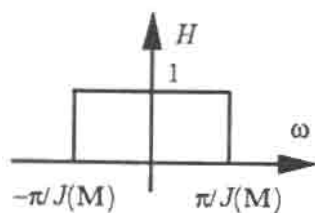


Figure 3.4. The desired response of the 1D filter $H(\omega)$.

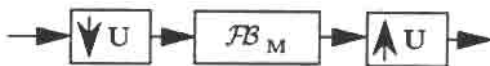


Figure 3.5. Pertaining to the illustration of the unimodular transformation.

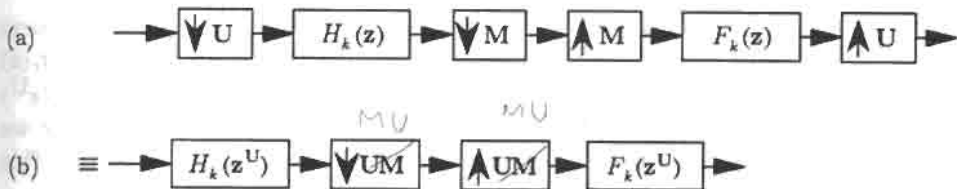


Figure 3.6. Derivation of the k th subband of the new system \mathcal{FB}_{UM} .

decimation, $Y(\mathbf{w})$ has support $SPD(\frac{\pi}{J(\hat{\mathbf{M}})}\hat{\mathbf{M}}^T)$, which is the same as $SPD(\pi\mathbf{M}^{-T})$ (by the definition of $\hat{\mathbf{M}}$). So $P(\mathbf{w})$ with support $SPD(\pi\mathbf{M}^{-T})$ can be design through the following procedures.

1. Design a 1D filter $H(\omega)$ with desired response as in Fig. 3.4. Define $h_s(\mathbf{n}) = h(n_0)h(n_1) \cdots h(n_{D-1})$, where $h(n)$ is the impulse response of $H(\omega)$. Then $H_s(\mathbf{w})$ has support $SPD(\frac{\pi}{J(\hat{\mathbf{M}})}\mathbf{I})$.
2. Let $P(\mathbf{w})$ be the $\hat{\mathbf{M}}$ -fold decimated version of $H_s(\mathbf{w})$, i.e., $p(\mathbf{n}) = h_s(\hat{\mathbf{M}}\mathbf{n})$. Then $P(\mathbf{w})$ has support $SPD(\pi\mathbf{M}^{-T})$.

Remark. It can be verified that the filters designed through the preceding approach have separable polyphase components. In this case, if $E_i(\mathbf{w})$ are the polyphase components of $P(\mathbf{w})$ as in (3.1), then $E_i(\mathbf{w})$ is separable and can be expressed as the product of polyphase components of the 1D filter $h(n)$. So the complexity of the DFT filter bank implementation in Fig. 3.2 grows linearly with the number of dimensions.

3.2. Unimodular Transformation [49]

Consider the D -dimensional filter bank with integer decimation matrix \mathbf{M} in Fig. 1.1. This filter bank will be denoted by $\mathcal{FB}_{\mathbf{M}}$. Suppose the filter bank has perfect reconstruction. Recall that a $D \times D$ unimodular decimator \mathbf{U} or a unimodular expander \mathbf{U} only permutes the input. So if we insert a decimator \mathbf{U} before the filter bank $\mathcal{FB}_{\mathbf{M}}$ and an expander \mathbf{U} after $\mathcal{FB}_{\mathbf{M}}$ (Fig. 3.5), the new system still has perfect reconstruction. This is equivalent to inserting a decimator \mathbf{U} before the analysis filter and an expander \mathbf{U} after the synthesis filter in each subband (Fig. 3.6(a)). We can redraw Fig. 3.6(a) as Fig. 3.6(b). Denote the new filter bank with decimation matrix \mathbf{UM} by $\mathcal{FB}_{\mathbf{UM}}$. The system $\mathcal{FB}_{\mathbf{UM}}$ will be called the unimodular transformation of $\mathcal{FB}_{\mathbf{M}}$ by \mathbf{U} . The k th analysis filter and the k th synthesis filter

of $\mathcal{FB}_{\mathbf{UM}}$ are respectively $H_k(\mathbf{z}^{\mathbf{U}})$ and $F_k(\mathbf{z}^{\mathbf{U}})$. If the analysis filter $H_k(\mathbf{z})$ in the original filter bank $\mathcal{FB}_{\mathbf{M}}$ has support S_k , the analysis filter $H_k(\mathbf{z}^{\mathbf{U}})$ in the new system $\mathcal{FB}_{\mathbf{UM}}$ has support $\mathbf{U}^{-T} S_k$ given by

$$\mathbf{U}^{-T} S_k = \{\mathbf{U}^{-T} \mathbf{w}, \mathbf{w} \in S_k\}.$$

Now consider the special case when the original filter bank is a 2D separable system with $\mathbf{M} = \Lambda$, where Λ is a 2×2 diagonal matrix. Then each analysis filter $H_k(\mathbf{z})$ consists of four shifts of $SPD(\frac{\pi}{2} \Lambda^{-1})$. For the system $\mathcal{FB}_{\mathbf{U}\Lambda}$, the analysis filter $H_k(\mathbf{z}^{\mathbf{U}})$ consists of four shifts of $SPD(\frac{\pi}{2} \mathbf{U}^{-T} \Lambda^{-1})$. So, using the unimodular transformation we can design nonseparable PR filter banks $\mathcal{FB}_{\mathbf{U}\Lambda}$ from separable PR filter banks \mathcal{FB}_{Λ} . This is demonstrated by the following design example.

Example 3.1. Unimodular transformation. Let $\Lambda = \begin{pmatrix} 4 & 0 \\ 0 & 5 \end{pmatrix}$. We can design a separable 20-channel filter bank \mathcal{FB}_{Λ} with decimation matrix Λ by concatenating a 1D four-channel filter bank and a 1D five-channel filter bank. Let $\mathcal{FB}_{\mathbf{U}\Lambda}$ be the unimodular transformation of \mathcal{FB}_{Λ} by \mathbf{U} , where $\mathbf{U} = \begin{pmatrix} 2 & -1 \\ -1 & 1 \end{pmatrix}$, then $\mathcal{FB}_{\mathbf{U}\Lambda}$ is nonseparable. Supports of some of the analysis filters in $\mathcal{FB}_{\mathbf{U}\Lambda}$ are shown in Fig. 3.7(a). Fig. 3.7(b) shows the magnitude response of the lowpass analysis filter.

3.3. Unimodular Transformation and Two-Channel Filter Banks

Recall the two-channel filter banks with parallelogram-supported filters as in Fig. 1.7. It can be verified that the supports of the lowpass analysis or synthesis filters in those four cases of Fig. 1.7 are of the form $SPD(\pi \mathbf{M}_i^{-T})$, with $\mathbf{M}_i = \mathbf{U}_i \mathbf{Q}$, where \mathbf{U}_i are unimodular and \mathbf{Q} is the quincunx matrix in Fig. 1.2. The matrix \mathbf{U}_i for the cases (a), (b), (c) and (d) are respectively

$$\mathbf{U}_1 = \begin{pmatrix} 1 & -1 \\ 0 & 1 \end{pmatrix}, \mathbf{U}_2 = \begin{pmatrix} -1 & 1 \\ 0 & 1 \end{pmatrix}, \mathbf{U}_3 = \begin{pmatrix} 0 & -1 \\ 1 & -1 \end{pmatrix}, \mathbf{U}_4 = \begin{pmatrix} 0 & 1 \\ 1 & -1 \end{pmatrix}.$$

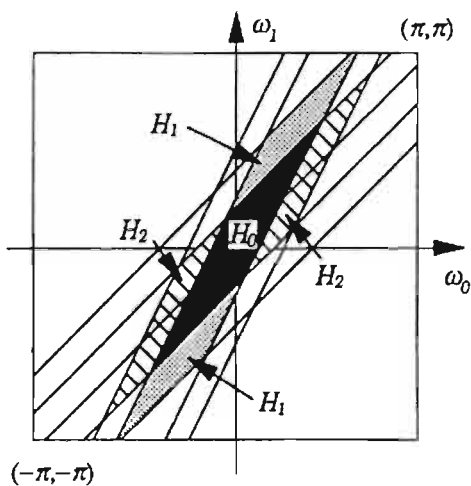
We can choose the decimation matrix to be \mathbf{M}_i . Since $\mathbf{M}_i = \mathbf{U}_i \mathbf{Q}$, where \mathbf{U}_i are unimodular, these filter banks can be derived from the diamond filter bank. Thus, these systems are unimodular transformations of the diamond filter bank.

It can be shown that any 2×2 integer matrix \mathbf{M} with $|\det \mathbf{M}| = 2$ can be expressed as one of the following three forms

$$\mathbf{M} = \mathbf{U} \begin{pmatrix} 1 & 0 \\ 0 & 2 \end{pmatrix}, \mathbf{M} = \mathbf{U} \begin{pmatrix} 2 & 0 \\ 0 & 1 \end{pmatrix} \text{ or } \mathbf{M} = \mathbf{U} \mathbf{Q},$$

where \mathbf{Q} is the quincunx matrix. So the corresponding two-channel filter bank with parallelogram supports can always be obtained as the unimodular transformation of the diamond filter bank or the unimodular transformation of 1D filter banks. In the quadrant filter bank

(a)



(b)

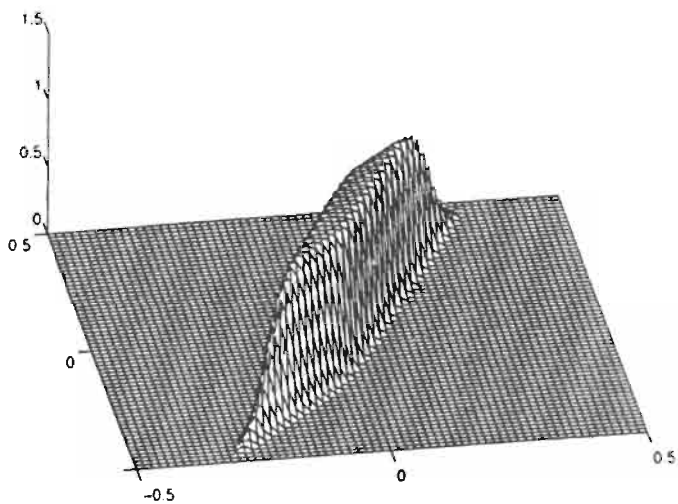


Figure 3.7. Example 3.1. Unimodular transformation. (a) Spectral supports of some of the analysis filters and (b) the magnitude response of the low-pass analysis filter with frequency normalized by 2π .

(Fig. 1.5), supports of the analysis filters are not parallelograms; the quadrant filter bank can not be obtained as the unimodular transformation of the diamond filter bank or 1D filter banks.

3.4. MD Filter Banks from 1D Filter Banks by using Transformation

In Sec. II, we designed the two-channel diamond filter bank from a 1D two-channel filter bank by use of McClellan transformation. The more general subject of 1D M -channel to MD M -channel transformations has been studied by Shah and Kalker in [43]. In particular, the results given below are shown therein.

Suppose that a 1D M -channel filter bank \mathcal{FB}_M has perfect reconstruction with distortion function $T(z) = 1$. The analysis and synthesis filters are denoted respectively by $H_k(z)$ and $F_k(z)$. Let \mathbf{N} be a $D \times D$ integer matrix with $J(\mathbf{N}) = M$ and let $K(\mathbf{z})$ be a 1D scalar function of $\mathbf{z} = (z_0 \ z_1 \ \dots \ z_{D-1})^T$. Let $\mathcal{FB}_{\mathbf{N}}$ be a D -dimensional filter bank with decimation matrix \mathbf{N} , analysis filters $H'_k(\mathbf{z}) = H_k(K(\mathbf{z}))$ and synthesis filters $F'_k(\mathbf{z}) = F_k(K(\mathbf{z}))$. One can show that $\mathcal{FB}_{\mathbf{N}}$ has perfect reconstruction if the following two conditions hold.

1. The decimation matrix \mathbf{N} has Smith form decomposition $\mathbf{N} = \mathbf{U}\mathbf{\Lambda}\mathbf{V}$ (see Sec. 1.3 for a review of Smith form decomposition), where $\mathbf{\Lambda}$ is of the form

$$\mathbf{\Lambda} = \begin{pmatrix} 1 & 0 & & 0 \\ 0 & 1 & & 0 \\ \vdots & & \ddots & \vdots \\ 0 & 0 & & M \end{pmatrix}. \quad (3.3)$$

2. The transformation $K(\mathbf{z})$ is of the form $K(\mathbf{z}) = \mathbf{z}^{-\mathbf{U}(0 \ 1)^T} \widehat{K}(\mathbf{z}^{\mathbf{N}})$, for some $\widehat{K}(\mathbf{z})$.

Remarks.

1. The original statement of the first condition in [43] is that the vectors in $\mathcal{N}(\mathbf{N})$ form a cyclic group under modulo \mathbf{N} . However as shown in [8], this condition is equivalent to the statement that \mathbf{N} has the special Smith form as given in (3.3). Also the original statement of the second condition in [43] is that $K(\mathbf{z})$ is of the form $K(\mathbf{z}) = \mathbf{z}^{-\mathbf{d}} \widehat{K}(\mathbf{z}^{\mathbf{N}})$, where \mathbf{d} is a group generator of $\mathcal{N}(\mathbf{N})$. But it follows from (3.3) that $\mathbf{U}(0 \ 1)^T$ is a group generator of $\mathcal{N}(\mathbf{N})$.
2. The supports of the D -dimensional analysis and synthesis filters are governed by the transformation $K(\mathbf{z})$ and the choice of \mathbf{N} . As perfect reconstruction is preserved in the transformation described above, only the transformation $K(\mathbf{z})$ remains to be designed. For the filter bank with diamond filters, the McClellan transformation is appropriate for realizing the 2D diamond filters. However, except in this case, there is no systematic approach of finding the transformation $K(\mathbf{z})$ that controls the shape of the 2D (more generally, D dimensional) analysis and synthesis filters. In general, the transformation $K(\mathbf{z})$ does not faithfully translate the characteristics of 1D filters. So even if the

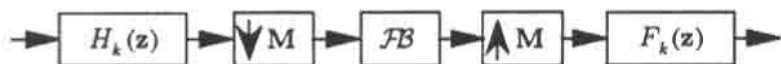


Figure 4.1. Derivation of perfect reconstruction tree structured filter bank.

1D analysis and synthesis filters in \mathcal{FB}_M have good stopband attenuation and good passbands, the D -dimensional analysis and synthesis filters resulting from the previous formulation may not have these properties.

4. Tree Structured Filter Banks

Consider the filter bank in Fig. 1.1. In the k th subband, we can insert another filter bank \mathcal{FB} (Fig. 4.1) to obtain a tree-structured filter bank. If the filter bank in Fig. 1.1 has perfect reconstruction (PR) and \mathcal{FB} is also PR with distortion function $T(\mathbf{z}) = 1$, the overall system remains PR. In this case, we say that the filter bank in Fig. 1.1 is the first level of the tree and \mathcal{FB} is the second level. Repeat this insertion of PR filter bank, we can obtain a tree structure of many levels. The separable systems are examples of tree-structured filter banks in which all the member filter banks are one-dimensional. In 2D, tree structure of some extensively-studied systems, e.g. the two-channel filter banks or the separable filter banks, sometimes offers very sophisticated supports.

Example 4.1. Directional filter banks [3]. The directional filter bank with supports as in Fig. 1.9 can be obtained by using a tree structure to cascade some commonly used two-channel systems. In particular, it can be obtained by cascading filter banks with fan filters (Fig. 1.6) and filter banks with supports as in Fig. 1.7 (except some minor modifications). We will explain in detail how to obtain $H_0(\mathbf{z})$ and $H_1(\mathbf{z})$ in Fig. 1.9. The supports of other analysis filters can be obtained in a similar manner. Consider the tree structure in Fig. 4.2. Let the analysis filters $G_0(\mathbf{z})$ and $G_1(\mathbf{z})$ have fan supports as in Fig. 1.6. Also let the support of $K_0(\mathbf{z})$ and $K_1(\mathbf{z})$ be as in Fig. 4.3, which are shifts of the parallelograms in Fig. 1.7(a) by $(\pi \ \pi)^T$. By use of Noble identities (Sec. 1.3), Fig. 4.2 can be redrawn as Fig. 4.4. The filters $G_0(\mathbf{z}^{\mathbf{Q}})$, $K_0(\mathbf{z}^{2\mathbf{I}_2})$ and $K_1(\mathbf{z}^{2\mathbf{I}_2})$ respectively have supports shown in Fig. 4.5. So $G_0(\mathbf{z})G_0(\mathbf{z}^{\mathbf{Q}})K_0(\mathbf{z}^{2\mathbf{I}_2})$ and $G_0(\mathbf{z})G_0(\mathbf{z}^{\mathbf{Q}})K_1(\mathbf{z}^{2\mathbf{I}_2})$ yield the desired support for $H_0(\mathbf{z})$ and $H_1(\mathbf{z})$.

Example 4.2. Consider the hexagon matrix $\mathbf{M} = \begin{pmatrix} 1 & 1 \\ -2 & 2 \end{pmatrix}$, which can be factorized as

$$\mathbf{M} = \begin{pmatrix} 1 & 0 \\ 0 & 2 \end{pmatrix} \begin{pmatrix} 1 & 1 \\ -1 & 1 \end{pmatrix}.$$

Suppose the first level of the tree is a separable system as in Fig. 1.3(b) and the second level is the diamond filter bank (Fig. 1.4). Then the four analysis filters of the overall system have supports as shown in Fig. 4.6.

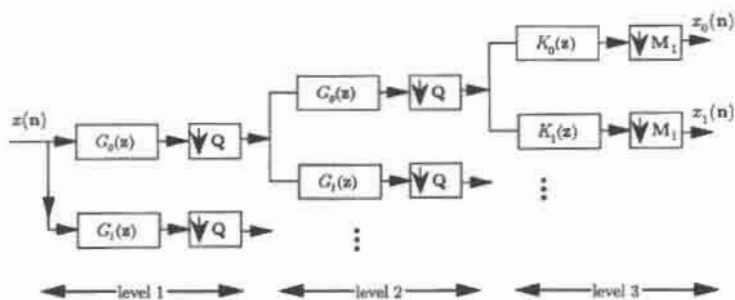


Figure 4.2. Tree-structured filter bank for the derivation of directional filter banks. In the first and second levels, each subband is split into two. Only the first two subbands of the overall system are shown in the figure.

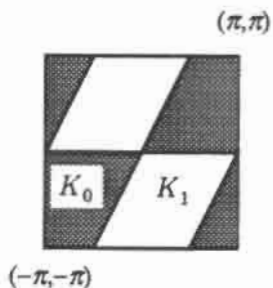


Figure 4.3. The support of the filters $K_0(z)$ and $K_1(z)$.

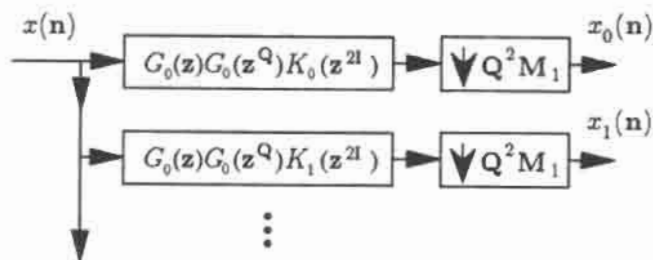


Figure 4.4. The equivalent parallel structure of Fig. 4.2.

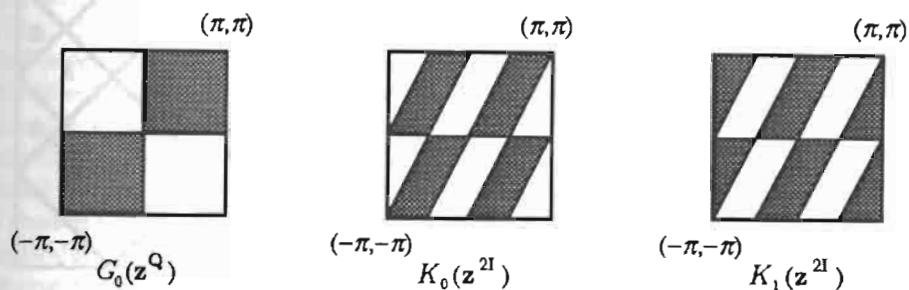


Figure 4.5. The supports of $G_0(z^Q)$, $K_0(z^{2I})$ and $K_1(z^{2I})$.

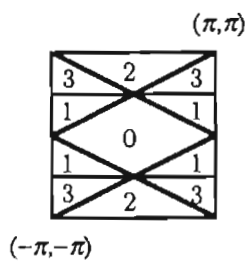


Figure 4.6. Example 4.2. Tree structured filter bank. The supports of the analysis filters. In the figure the support of $H_k(z)$ is denoted by k .

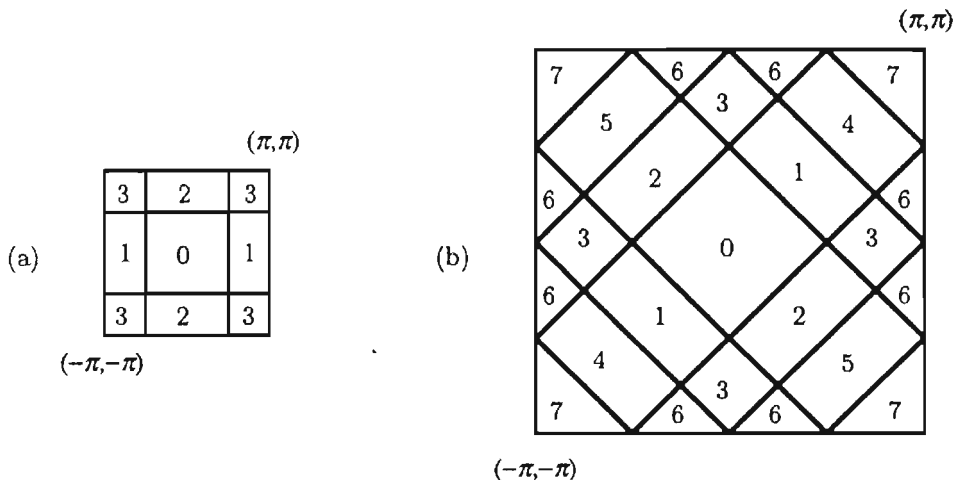


Figure 4.7. Example 4.3. Tree structured filter bank. (a) The first level of the tree: the four-channel separable filter bank. The supports of the four separable analysis filters (with the support of the k th filter denoted by k). (b) The supports of the eight analysis filters in the overall system. The support of $H_k(z)$ is denoted by k .

Example 4.3. Let

$$\mathbf{M} = \begin{pmatrix} 1 & 1 \\ -1 & 1 \end{pmatrix} \begin{pmatrix} 2 & 0 \\ 0 & 2 \end{pmatrix}.$$

If we use the diamond filter bank (Fig. 1.4) for the first level of the tree. For the second level, we use a separable system with decimation matrix $2\mathbf{I}_2$ (Fig. 4.7(a)), which can be obtained as a tree structure of two 1D two-channel filter banks. Then the resulting analysis filters of the overall system have supports as shown Fig. 4.7(b). Each analysis filter consists of four parallelograms.

5. Two-Dimensional Cosine Modulated Filter Banks: Basic Consideration

We first recall the main features of one-dimensional (1D) cosine modulated filter banks (CMFB). The process of constructing 1D CMFB will give us a general idea of the procedures for constructing 2D CMFB. The experience with 1D CMFB will help also us gain some insight to foresee the difficulties in constructing the 2D CMFB.

5.1. One-Dimensional Cosine Modulated Filter Banks (CMFB)

5.1.1. Introduction

Two types of cosine modulated filter banks have been developed, pseudo QMF systems [10], [41], [37] and perfect reconstruction systems [39], [35], [26]. Consider the filter bank in Fig. 1.1, in which the decimation matrix is a scalar M . An M -channel CMFB (pseudo-QMF or perfect reconstruction) is typically obtained by starting from a $2M$ channel uniform DFT filter bank, [50]. Each filter in the DFT filter bank is a shifted version of a lowpass prototype $P(\omega)$ (Fig. 5.1(a)) with bandwidth π/M , which is half the total bandwidth of each filter in the desired M -channel system. The filters in the DFT filter bank are then shifted by $\pi/2M$ and paired to obtain real-coefficient analysis filters as in Fig. 5.1(b) for the M channel CMFB. The shifts of the prototype are denoted by $P_k(\omega)$ in the figure. The total bandwidth of each of the analysis filters in the CMFB is $2\pi/M$, which is two times that of the prototype. In almost all the designs, the synthesis filters are time-reversed versions of the corresponding analysis filters; the analysis and synthesis filters have the same spectral support.

In the CMFB described above, as each analysis filter consists of two shifted copies of the prototype, each of the two copies has $M - 1$ images due to decimation followed by expansion. By construction, the images of the analysis filters are adjacent to the support of the corresponding synthesis filters but are not overlapping with the passbands of synthesis filters as shown in Fig. 5.1(c). Thus, if the prototype filter is an ideal brick-wall filter, there is no aliasing and in this case the filter bank has perfect reconstruction. If the prototype filter is not ideal, those images that are adjacent to the synthesis filter result in major aliasing (Fig. 5.1(d)) while those that are not adjacent to the synthesis filters will be attenuated to the stopband level of the prototype filter. In the pseudo QMF CMFB, only the major aliasing errors are canceled and approximate alias cancellation is attained. Approximate reconstruction is then achieved without sophisticated optimization of the lowpass prototype. In the perfect reconstruction CMFB, the prototype is further optimized under the constraint that the CMFB is paraunitary, hence perfect reconstruction is assured. The paraunitariness of the CMFB is guaranteed if the polyphase components of the prototype filter satisfy some pairwise power complementary conditions [26]. In both pseudo QMF and perfect reconstruction systems, the design of the whole filter bank is reduced to the optimization of the lowpass prototype filter. The complexity of the analysis bank is equal to that of a prototype filter plus a DCT matrix.

5.1.2. General setting and main features of 1D CMFB

From the above discussion of 1D CMFB, we observe that the general setting of 1D M -channel CMFB can be summarized as follows.

1. Construct a $2M$ -channel uniform DFT filter bank.
2. Shift the filters in the DFT filter bank by $\pi/2M$ and combine appropriate pairs of filters to yield real-coefficient analysis filters.

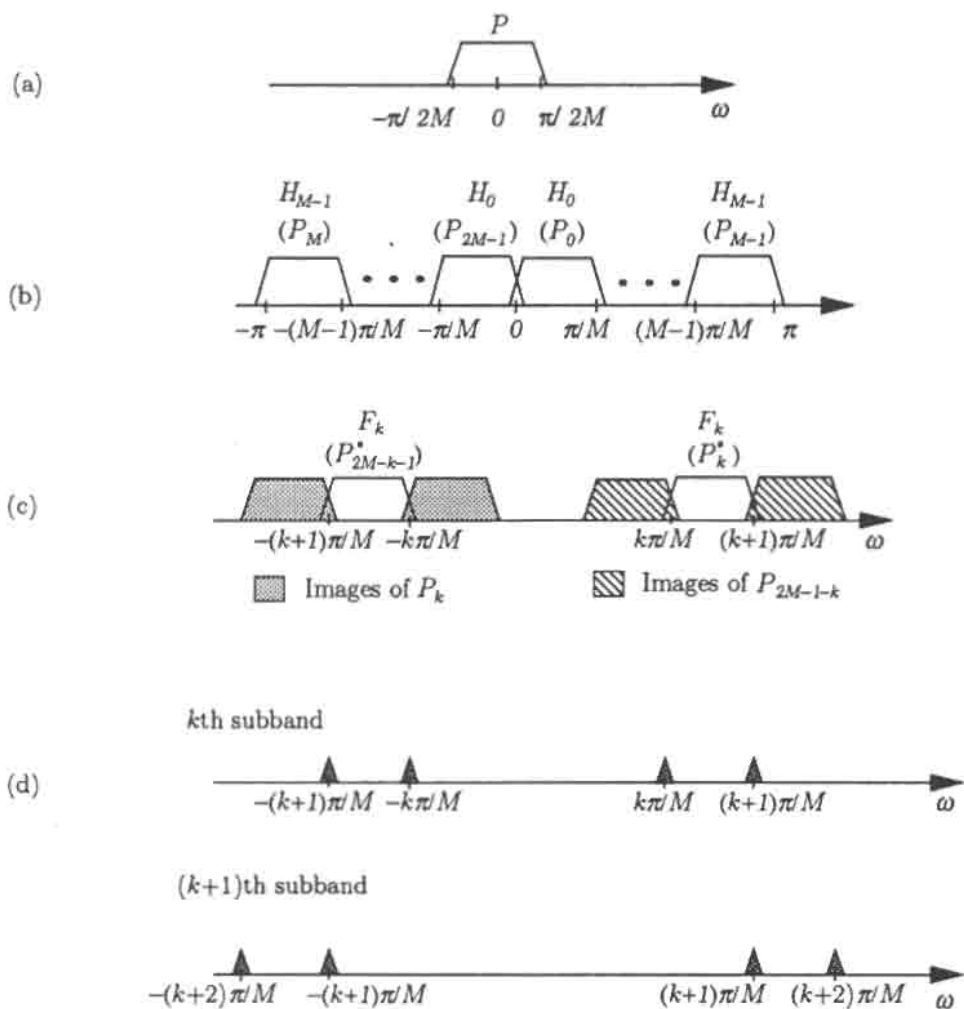


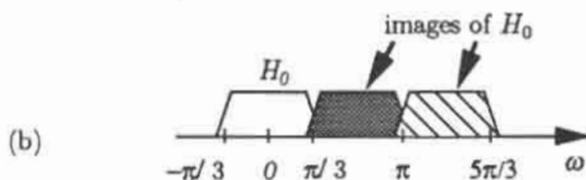
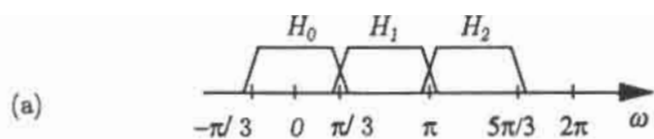
Figure 5.1. One-dimensional cosine modulated filter bank. (a) The support of the prototype filter $P(\omega)$. (b) The support of the analysis filters $H_k(\omega)$. Each analysis filter has two parts, $P_k(\omega)$ and $P_{2M-1-k}(\omega)$. (c) Images of the analysis filter $H_k(\omega)$ that are adjacent to the synthesis filter $F_k(\omega)$. (d) The major aliasing in the k th subband and the $(k+1)$ th subband.

Main features of 1D CMFB. The support configuration of the 1D CMFB constructed above has the following two features. (1) The support configuration satisfies the **bandpass sampling criterion**: images of the analysis filter passbands do not overlap with passbands of the synthesis filters. Furthermore, the filter bank has perfect reconstruction when the analysis and synthesis filters are ideal brick-wall filters. (2) When the filters are not ideal, the major aliasing errors that contribute to the same aliasing transfer function $A_i(\mathbf{w})$ appear in pairs. For example, both k th and $(k+1)$ th subbands have major aliasing errors around the frequency $k\pi/M$ (Fig. 5.1(d)) and it can be verified that these two aliasing errors contribute to the same aliasing transfer function $A_k(\mathbf{w})$. A support configuration without this feature will be referred to as *nonpermissible*. The importance of satisfying the sampling criterion and the significance of support permissibility are addressed next.

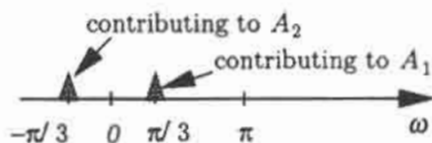
Satisfying the sampling criterion. This feature is indispensable for the design of perfect reconstruction filter banks. For a configuration that does not satisfy the sampling criterion, severe aliasing will be created in the subbands no matter how good the filters are. A filter bank with a configuration that violates the sampling criterion can not have perfect reconstruction even if the analysis and synthesis filters are ideal brick-wall filters.

Support permissibility. Support permissibility allows the possibility of cancellation of major aliasing. Pairwise major aliasing terms are necessary if cancellation of major aliasing is to take place. For a filter bank with a nonpermissible support configuration, the filters can not have good stopband attenuation [8]. The reason is as follows. Suppose a perfect reconstruction filter bank has a nonpermissible support configuration and the individual filters have good stopband attenuation. Then, major aliasing terms do not appear in pairs and can not be cancelled. This contradicts the fact that the filter bank has perfect reconstruction. Therefore, a PR filter bank with nonpermissible support configuration can not have filters with good stopband attenuation except in the case that all the filters are ideal brick-wall filters.

Example of nonpermissible support. The configuration of the DFT filter bank is an example of nonpermissible support. The DFT filter bank has the first feature of 1D CMFB (i.e. satisfying the bandpass sampling criterion) but not the second one. As a result, the individual analysis and synthesis filters in a perfect reconstruction DFT filter bank can not have good attenuation unless all the filters are ideal brick-wall filters. To see this, consider a three-channel DFT filter bank. The supports of the analysis filter are as shown in Fig. 5.2(a). The subband signals are decimated by 3 and expanded by 3, so each analysis filter has two images. For example, the images of $H_0(z)$ are as shown in Fig. 5.2(b). The analysis filter $H_k(z)$ and its images do not overlap in the passbands. If the prototype filter is ideal, no aliasing is created in the subbands and the filter bank has perfect reconstruction. So the support configuration of the DFT filter bank satisfies the sampling criterion and has the first feature of the CMFB. When the filters have good stopband attenuation, the major aliasing errors result from the two images of $H_0(z)$ are shown in Fig. 5.2(c). The aliasing around the frequency $\pi/3$ contribute to the alias transfer function $A_1(z)$ while the aliasing error around the frequency $-\pi/3$ contribute to the alias transfer function $A_2(z)$. Similar aliasing errors occur in the other two subbands as well (Fig. 5.2(c)). We observe that around the frequency $\pi/3$, both the first and the second subband have aliasing errors. However, these two aliasing errors contribute to different aliasing transfer functions and can not cancel



(c) first subband



second subband

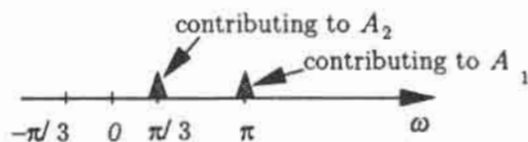


Figure 5.2. Three-channel DFT filter bank. (a) The supports of the three analysis filters. (b) Images of $H_0(\omega)$ due to 3-fold decimation followed by 3-fold expansion. (c) Major aliasing in the first and second subbands.

each other. So for the DFT filter bank, aliasing can not be cancelled if the individual filters have good attenuation but are not ideal filters. In a perfect reconstruction filter bank, aliasing eventually has to be cancelled. We hence conclude that the filters in the perfect reconstruction DFT filter bank can not have good stopband attenuation except in the case when the filters are ideal.

5.2. Construction of Two-Dimensional Cosine Modulated Filter Bank

The separable 2D CMFB can always be obtained through concatenation of two 1D CMFB in the form of a tree [50]. Our interest in this paper is designing a nonseparable 2D CMFB. The prototype filter is in general a nonseparable 2D filter. Each analysis and synthesis filter is a cosine modulated version of the prototype and is also nonseparable. In the separable 2D CMFB case, each individual filter consists of four shifts of a separable 2D prototype. However, the real-coefficient constraint on the analysis filters requires only two copies of the prototype. We can therefore conceive that in the more general case the individual filters can have two or four shifted copies of the prototype. In this paper, we study two classes of 2D FIR paraunitary cosine modulated filter banks: the two-copy CMFB and the four-copy CMFB. In the two-copy CMFB, each individual filter contains two shifted copies of the prototype and in the four-copy CMFB, each individual filter contains four shifted copies of the prototype. The filter bank will eventually be constrained to be paraunitary; the analysis filter $H_k(\mathbf{w})$ and the corresponding synthesis filter $F_k(\mathbf{w})$ are then related by $F_k(\mathbf{w}) = H_k^*(\mathbf{w})$ for perfect reconstruction. The analysis and synthesis filters have the same spectral support. Note that the two-copy CMFB is fundamentally different from a 2D separable CMFB obtained from two 1D CMFB. But the four-copy CMFB will reduce to separable 2D CMFB in special cases. Both of these systems are elaborated below.

Two-copy CMFB. Consider the filter bank in Fig. 1.1 with decimation matrix \mathbf{M} , non-diagonal in general. There are $|\det \mathbf{M}|$ channels since each decimator creates a decimation of $|\det \mathbf{M}|$. For a given $|\det \mathbf{M}|$ -channel filter bank as in Fig. 1.1, we start from a $2|\det \mathbf{M}|$ -channel uniform 2D DFT filter bank [50]. Every filter in the DFT filter bank is a shifted version of a lowpass FIR (non-rectangular) prototype. The prototype has a parallelogram support, so every filter in the DFT filter bank has a parallelogram support. The filters in the DFT filter bank are shifted and paired to obtain real-coefficient analysis filters. Each analysis filter is then a cosine modulated version of the prototype and each analysis filter consists of two shifted copies of the prototype. All the analysis and synthesis filters have real coefficients. We then examine whether the supports of the analysis and synthesis filters satisfy the sampling criterion. Namely, the images of the analysis filter passbands should not overlap with passbands of the synthesis filters. Under this condition we study the sufficient conditions such that cancellation of major aliasing (due to overlapping transition bands) can be structurally enforced. Finally, having cancelled the major aliasing, we constrain the prototype to ensure perfect reconstruction of the two-copy CMFB.

Four-copy CMFB. The four-copy CMFB will be constructed in a similar way. But in the four-copy case, we design a $4|\det \mathbf{M}|$ -channel uniform DFT filter bank. Then we shift the filters in the DFT filter bank and combine four shifted filters to obtain real-coefficient

analysis filters for the four-copy CMFB. The rest of the construction procedure is the same as that of two-copy CMFB.

The above construction of two-copy and four-copy CMFB is an immediate imitation of 1D CMFB. The more refined construction procedures are listed below.

1. General setting. To complete the general setting of the 2D CMFB, we need to answer the following questions first. For a given filter bank with decimation matrix \mathbf{M} as in Fig. 1.1, how to construct the uniform DFT filter bank? How to shift the filters in the DFT filter bank and obtain the analysis filters such that the support configuration of the 2D CMFB is an extension of 1D version? In 1D case, there is only one way to shift the filters of the DFT filter bank. Do we have more variety in 2D case?

2. Ideal case. Having completed the general setting of 2D CMFB, we proceed to examine the support configuration of 2D CMFB. We first check whether the configuration has the first feature of 1D CMFB. The configuration should be such that the bandpass sampling criterion is satisfied and the filter bank has perfect reconstruction in the case of ideal filters. To satisfy the sampling criterion, the images of passbands of an analysis filter should not overlap with passbands of the corresponding synthesis filter.

3. Support permissibility and alias cancellation. For those that satisfy the sampling criterion, we examine support permissibility. Permissibility of a support configuration means that cancellation of major aliasing is possible. If a support configuration is permissible, we further study how to cancel major aliasing.

4. Perfect reconstruction. Having cancelled major aliasing, we then constrain the prototype to achieve perfect reconstruction as in the case of 1D CMFB.

6. Two-Copy Cosine Modulated Filter Banks

6.1. General Setting of Two-Copy CMFB

1. Uniform DFT filter bank. To design a two-copy CMFB with decimation matrix \mathbf{M} , we start from a uniform DFT filter bank [50] with decimation matrix $\mathbf{N} = \mathbf{ML}$, where \mathbf{L} is an integer matrix (to be chosen appropriately) with $|\det \mathbf{L}| = 2$. For example, let

$$\mathbf{M} = \begin{pmatrix} 7 & -2 \\ 0 & 1 \end{pmatrix} \quad \text{and} \quad \mathbf{L} = \begin{pmatrix} 1 & 1 \\ 2 & 4 \end{pmatrix}, \quad \text{then} \quad \mathbf{N} = \begin{pmatrix} 3 & -1 \\ 2 & 4 \end{pmatrix}.$$

The supports of the individual filters $\{P_k(\mathbf{w}), 0 \leq k \leq 13\}$ in the DFT filter bank are as shown in Fig. 3.1. Each filter in the DFT filter bank is a shifted version of the prototype $P(\mathbf{w})$, which has a parallelogram support $SPD(\pi\mathbf{N}^{-T})$. For a given \mathbf{M} , the support of the prototype is different for different choice of \mathbf{L} .

2. The analysis and synthesis filters. In 1D CMFB, we shift the filters in the DFT filter bank by $\pi/2M$. But in 2D case, the shifts are vector-shifts. We can shift the filters in the DFT filter bank in three possible directions as in Fig. 6.1. The result supports with respect to the three different shifts are shown in Fig. 6.2(a)–(c). For all the three cases, filters can be paired to obtain real-coefficient analysis filters for the two-copy CMFB. For example, in Fig. 6.2(a), the filter coefficients of $Q_{A,i}(\mathbf{w})$ and $Q'_{A,i}(\mathbf{w})$ are complex conjugates of each

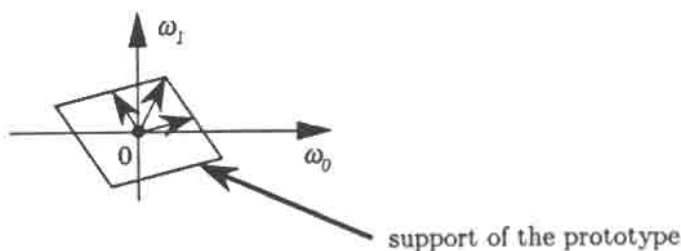


Figure 6.1. Three possible vector shifts.

other and can be paired to obtain the analysis filter,

$$H_{A,i}(\mathbf{w}) = Q_{A,i}(\mathbf{w}) + Q'_{A,i}(\mathbf{w}). \quad (6.1)$$

The corresponding synthesis filter is

$$F_{A,i}(\mathbf{w}) = Q_{A,i}^*(\mathbf{w}) + Q'_{A,i}^*(\mathbf{w}).$$

Similarly in Fig. 6.2(b), $Q_{B,i}(\mathbf{w})$ and $Q'_{B,i}(\mathbf{w})$ are combined to obtain the analysis filter $H_{B,i}(\mathbf{w})$ and in Fig. 6.2(c) $Q_{C,i}(\mathbf{w})$ and $Q'_{C,i}(\mathbf{w})$ are combined to obtain $H_{C,i}(\mathbf{w})$. Each analysis filter consists of two parallelograms. We observe that all three possible support configurations are extension of the 1D version. The three support configurations will be referred to as configurations A, B, and C. From Fig. 6.2 it seems that configurations A and B are very similar. Indeed as we will see in subsequent discussion, properties derived for configurations A are also true for configuration B except some minor modifications.

6.2. The Ideal Case

In the above general setting of two-copy CMFB, for a given decimation matrix \mathbf{M} , we first construct a DFT filter bank with decimation matrix $\mathbf{N} = \mathbf{M}\mathbf{L}$. The matrix \mathbf{L} is an integer matrix with determinant 2. No additional assumption has been made on \mathbf{L} . On the other hand, given a DFT filter bank with decimation matrix \mathbf{N} , we can always shift the filters in the DFT filter bank by the three different amounts indicated in Fig. 6.1. These three shifts gives us configurations A, B, and C. So the derivation of configurations A, B, and C does not relate to \mathbf{L} . However, we will see that for a given \mathbf{L} , not all three configurations can satisfy the bandpass sampling criterion. In particular, we will establish a connection between the lattice of \mathbf{L}^T and valid choice of configurations.

As \mathbf{L} has determinant 2, there are only three possible choices for $LAT(\mathbf{L}^T)$ as in Fig. 6.3(a)–(c). The lattice of \mathbf{L}^T is rectangular in Fig. 6.3(a),(b) and quincunx in Fig. 6.3(c). We will argue that for each configuration, there are only two choices of $LAT(\mathbf{L}^T)$ that can satisfy the sampling criterion and these combinations are the valid candidates for the development of two-copy CMFB. The relation between the three configurations and valid choice of $LAT(\mathbf{L}^T)$ is summarized in Table 6.1. In this case, when the sampling criterion

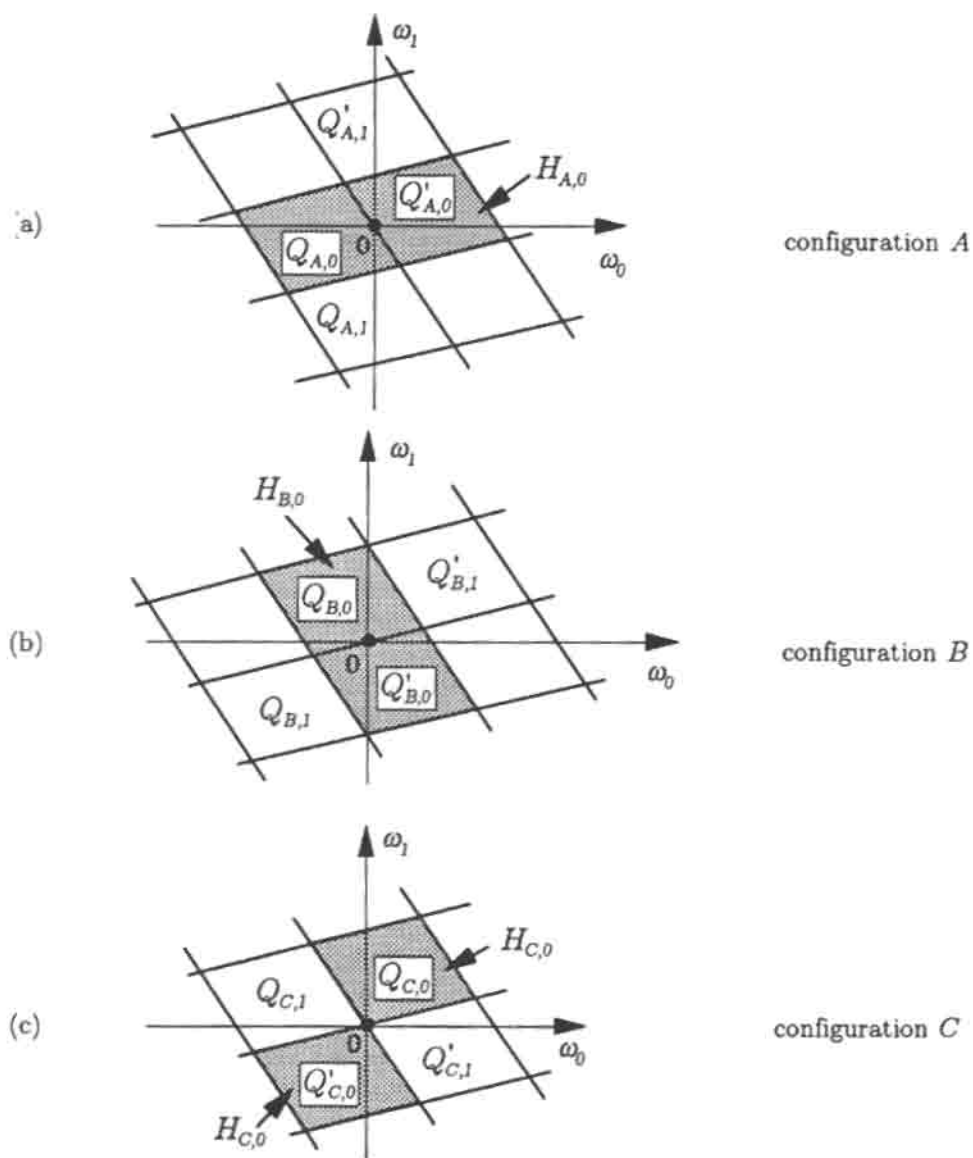
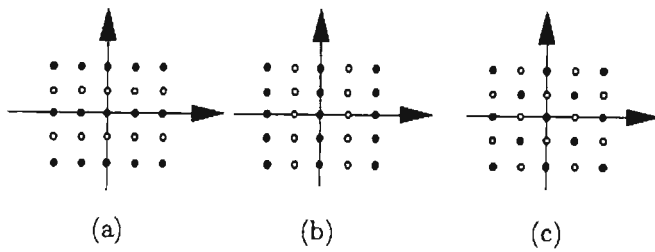


Figure 6.2. Three possible support configurations.



- Integers
- Integers on lattice of L^T

Figure 6.3. Possible lattices generated by L^T , when $|\det L| = 2$.

$LAT(L^T)$ configuration	lattice (a) (rectangular)	lattice (b) (rectangular)	lattice (c) (quincunx)
A		satisfied	satisfied
B	satisfied		satisfied
C	satisfied	satisfied	

Table 6.1. Possible combinations of configurations and $LAT(L^T)$ that satisfy the sampling criterion. Lattice (a)–(c) in the table are as in Fig. 6.3 (a)–(c).

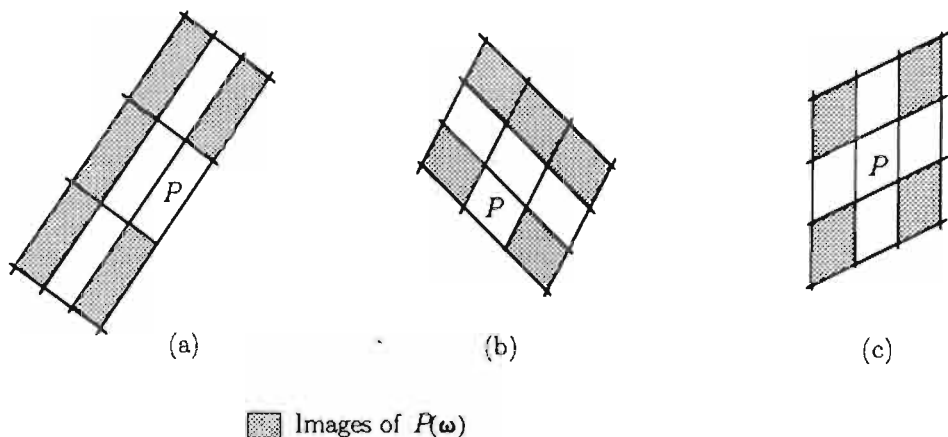


Figure 6.4. Images of the prototype $P(\mathbf{w})$ with respect to the three possible lattices generated by \mathbf{L}^T .

is satisfied, the filter bank has perfect reconstruction if the prototype is an ideal brick-wall filter. The remaining part of this subsection is devoted to the verification of Table 6.1.

To check whether a certain configuration satisfies the sampling criterion, it is essential to know exactly where the images of the analysis filters are located. As each analysis filter contains two shifted copies of the prototype, we first inspect the locations of images of $P(\mathbf{w})$ when it is decimated by \mathbf{M} and then expanded by \mathbf{M} . The images of $P(\mathbf{w})$ are [50]

$$P(\mathbf{w} - 2\pi\mathbf{M}^{-T}\mathbf{k}), \quad \mathbf{k} \in \mathcal{N}(\mathbf{M}^T) \quad \text{and} \quad \mathbf{k} \neq \mathbf{0}.$$

Recall that the support of $P(\mathbf{w})$ is $SPD(\pi\mathbf{N}^{-T})$, which depends on both \mathbf{M} and \mathbf{L} . For different $LAT(\mathbf{L}^T)$, $P(\mathbf{w})$ and its images form a certain pattern. In particular, it is a striped pattern in the case of rectangular $LAT(\mathbf{L}^T)$ and a check pattern in the case of quincunx $LAT(\mathbf{L}^T)$. For example, let $\mathbf{M} = \begin{pmatrix} 2 & 1 \\ -1 & 1 \end{pmatrix}$. When

$$\mathbf{L} = \begin{pmatrix} 1 & 0 \\ 0 & 2 \end{pmatrix}, \quad \mathbf{L} = \begin{pmatrix} 2 & 0 \\ 0 & 1 \end{pmatrix}, \quad \text{and} \quad \mathbf{L} = \begin{pmatrix} 1 & -1 \\ 1 & 1 \end{pmatrix},$$

the locations of the images are shown respectively in Fig. 6.4(a)–(c). In all three cases, images of $P(\mathbf{w})$ are confined to the grid formed by shifts of $P(\mathbf{w})$ in the DFT filter bank.

The lattice of \mathbf{L}^T and the sampling criterion

Configuration A. In what follows configuration A of Fig. 6.2(a) will be shown to satisfy the sampling criterion when $LAT(\mathbf{L}^T)$ is as in Fig. 6.3(b) and (c). For these two types of $LAT(\mathbf{L}^T)$, the filter bank has perfect reconstruction when the prototype is an ideal brick-wall filter. Consider the lowpass filter $H_{A,0}(\mathbf{w})$. When $LAT(\mathbf{L}^T)$ is rectangular as in

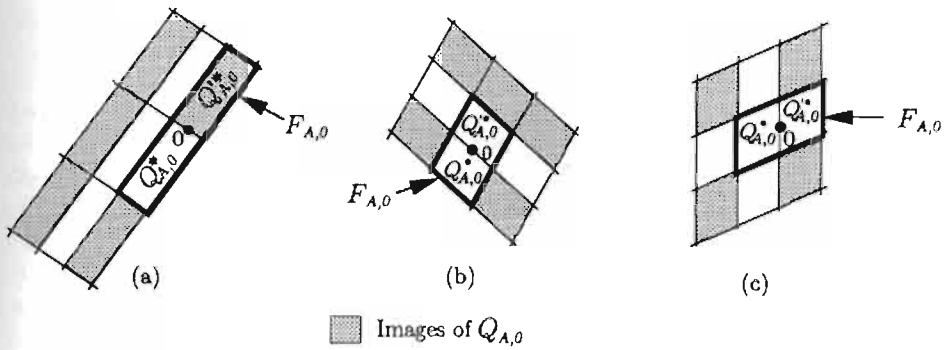


Figure 6.5. Configuration A and the sampling criterion. Images of $Q_{A,0}(\mathbf{w})$ with respect to the three different lattices generated by L^T .

Fig. 6.3(a), the support of $Q_{A,0}(\mathbf{w})$ and its images (shaded areas) are shown in Fig. 6.5(a). One image of $Q_{A,0}(\mathbf{w})$ completely falls on top of $Q'_{A,0}(\mathbf{w})$, which is part of the synthesis filter $F_{A,0}(\mathbf{w})$; the sampling criterion is not satisfied. When lattice of L^T is as in Fig. 6.3(b) or (c), the images of $Q_{A,0}(\mathbf{w})$ are shown in Fig. 6.5(b) and (c). In these two cases the images of $Q_{A,0}(\mathbf{w})$ are edge-adjacent to the synthesis filter $F_{A,0}(\mathbf{w})$ but not overlapping with $F_{A,0}(\mathbf{w})$. It can be verified that in every other subband, similar situation takes place: images of the analysis filters are adjacent to the synthesis filters but not overlapping with support of synthesis filters. Therefore, for the lattices of L^T shown in Fig. 6.3(b), (c), configuration A satisfies the sampling criterion.

Configuration B and C. Following a similar analysis, configuration B can be shown to satisfy the sampling criterion when $LAT(L^T)$ is as given in Fig. 6.3(a) and (c). Also configuration C can be shown to satisfy the sampling criterion when $LAT(L^T)$ is rectangular as given in Fig. 6.3(a) and (b). Moreover, in all these cases (configuration B or C) the filter bank has perfect reconstruction when the prototype is ideal.

6.3. Support Permissibility and Alias Cancellation

From the preceding analysis, we know that each of the three support configurations can satisfy the sampling criterion with two types of $LAT(L^T)$. Therefore there are six possible choices. If the prototype is an ideal brick-wall filter, perfect reconstruction can be achieved by any of the six choices. When the prototype is not ideal, aliasing will occur in the subbands. The six choices that satisfy the sampling criterion are not all valid candidates in terms of support permissibility [8]. However, in 2D case we have to be more careful in treating the notion of permissibility. We will consider a finer classification of support permissibility: edge-based permissibility and vertex-based permissibility.

Edge-based and vertex-based permissibility. Consider the analysis filter $H_{A,i}(\mathbf{w}) = Q_{A,i}(\mathbf{w}) + Q'_{A,i}(\mathbf{w})$ in configuration A. Suppose an image of $Q_{A,i}(\mathbf{w})$ or $Q'_{A,i}(\mathbf{w})$ is at any of the shaded areas (edge-adjacent to $Q'_{A,i}(\mathbf{w})$) in Fig. 6.6. If the prototype filter is

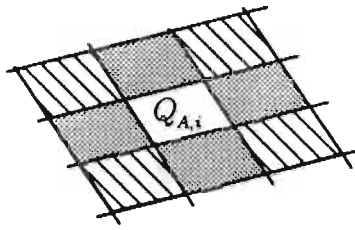
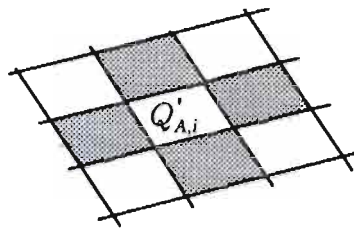


Figure 6.6. Pertaining to the illustration of support permissibility.

ideal, no aliasing is created. However, in practical cases the prototype filter is not ideal. Because of this edge-adjacent image, a considerable amount of edge-based aliasing will be created in the frequency region of the overlapping edges and this edge-based aliasing will add to the major aliasing. Cancellation of this edge-based aliasing is impossible if in the same frequency region there is no other edge-based aliasing error contributing to the same aliasing transfer function [8]. Whenever edge-based aliasing errors do not appear in pairs, the support configuration is called edge-based nonpermissible. Similar to the 1D case, we can argue that the filters in a PR filter bank can not have good stopband attenuation if the support configuration is edge-based nonpermissible. The 2D CMFB studied in [19] usually has this type of nonpermissible support. Similarly, when an image of $Q_{A,i}(\mathbf{w})$ or $Q'_{A,i}(\mathbf{w})$ is at any of the striped areas (vertex-adjacent to $Q^*_{A,i}(\mathbf{w})$) in Fig. 6.6, vertex-based aliasing will occur. If the vertex-based aliasing errors do not appear in pairs, the configuration is called vertex-based nonpermissible. Vertex-based nonpermissibility will also impose limitation on the stopband attenuation of the prototype. But the vertex-based aliasing is, however, not as serious as edge-based aliasing and vertex-based nonpermissibility is not as intolerable as edge-based nonpermissibility.

A simple test of support permissibility. From the general setting described in Sec. 6.1, we know how to obtain the analysis and synthesis filters from a DFT filter bank with twice the number of channels. The supports of the analysis and synthesis filters thus acquired are of a very regular nature. As a result, support permissibility of the two-copy CMFB can be tested through a very simple approach. Consider configuration *A* in Fig. 6.2. Notice that each analysis filter has two passbands, passband of $Q_{A,i}(\mathbf{w})$ and passband of $Q'_{A,i}(\mathbf{w})$. We can verify that except in special degenerate cases of N , support permissibility of the two-copy CMFB can be described as follows: if $Q_{A,i}(\mathbf{w})$ (or $Q'_{A,i}(\mathbf{w})$) is edge-adjacent to its own images, the configuration is edge-based nonpermissible. Similarly, if $Q_{A,i}(\mathbf{w})$ (or $Q'_{A,i}(\mathbf{w})$) is vertex-adjacent to its own images, the configuration is vertex-based nonpermissible. This testing rule of permissibility applies also to configurations *B* and *C*.

Rectangular $LAT(L^T)$: edge-based nonpermissible support. When $LAT(L^T)$ is rectangular as in Fig. 6.3(b), we observe that two images of $Q_{A,0}(\mathbf{w})$ are edge-adjacent to $Q_{A,0}(\mathbf{w})$ as shown by shaded areas in Fig. 6.5(a). So configuration *A* is in general not edge-based permissible with rectangular $LAT(L^T)$. Similarly, we can show that configuration *B*



■ Images of $Q_{A,i}$

Figure 6.7. Images of $Q_{A,i}(\mathbf{w})$ and their positions relative to $Q'_{A,i}(\mathbf{w})$; four images of $Q_{A,i}(\mathbf{w})$ are edge-adjacent to $Q'_{A,i}(\mathbf{w})$.

is not edge-based permissible with rectangular $LAT(L^T)$ in Fig. 6.3(a). As configuration C can satisfy the sampling criterion only for rectangular $LAT(L^T)$, configuration C is edge-based nonpermissible and hence not suitable for the development of two-copy CMFB.

Quincunx $LAT(L^T)$ and edge-based permissibility. Configuration A and B with quincunx $LAT(L^T)$. Consider configuration A first. Location of the images of $Q_{A,0}(\mathbf{w})$ is shown in Fig. 6.5(c). None of the images of $Q_{A,0}(\mathbf{w})$ are edge-adjacent to $Q_{A,0}(\mathbf{w})$. However, images of $Q_{A,0}(\mathbf{w})$ are vertex-adjacent to $Q_{A,0}(\mathbf{w})$. It can be verified that in every subband, the images of $Q_{A,i}(\mathbf{w})$ are vertex-adjacent to $Q_{A,i}(\mathbf{w})$ and images of $Q'_{A,i}(\mathbf{w})$ are vertex-adjacent to $Q'_{A,i}(\mathbf{w})$. In this case, configuration A has edge-based permissibility but lacks vertex-based permissibility.

On the other hand, note that images of $Q_{A,0}(\mathbf{w})$ are edge-adjacent to $Q'_{A,0}(\mathbf{w})$ and result in edge-based aliasing error. Similarly in every other subband, the images of $Q_{A,i}(\mathbf{w})$ are edge-adjacent to $Q'_{A,i}(\mathbf{w})$ and similar edge-based aliasing is created. In particular, it can be shown that four images of $Q_{A,i}(\mathbf{w})$ will be edge-adjacent to $Q'_{A,i}(\mathbf{w})$ as in Fig. 6.7. It turns out that these edge-based aliasing errors are in pairs and can actually cancel with one another if the linear-phase prototype satisfy some minor condition. To be more specific, let the impulse response of the prototype be $p(\mathbf{n})$ and

$$p(\mathbf{n}) = p(\mathbf{n}_s - \mathbf{n}), \text{ for some integer vector } \mathbf{n}_s. \quad (6.2)$$

Cancellation of above-described edge-based aliasing error will take place if

$$\mathbf{n}_s = \mathbf{N} \left(\begin{pmatrix} 0.5 \\ 0.5 \end{pmatrix} + \mathbf{d} \right), \text{ for some integer vector } \mathbf{d}. \quad (6.3)$$

This is a minor condition because it is always possible to shift the linear-phase prototype such that (6.3) is satisfied. We conclude that configuration A with quincunx $LAT(L^T)$ is free from edge-based aliasing if \mathbf{n}_s is as given in (6.3). Applying the preceding analysis on

configuration B (Fig. 6.2(b)) we can obtain a similar result: configuration B with quincunx $LAT(\mathbf{L}^T)$ is free from edge-based aliasing if the prototype satisfy the same condition (6.3).

Summary on the construction of the two-copy CMFB. In the above construction, we have set up the framework for two-copy CMFB. Following a very close analogy of 1D CMFB, we proposed the general setting of the two-copy CMFB. In the general setting, we started from a DFT filter bank with decimation matrix $\mathbf{N} = \mathbf{M}\mathbf{L}$ for a two-copy CMFB with decimation matrix \mathbf{M} . Then we derived configurations A , B and C . For the configurations to satisfy the sampling criterion, the choice of \mathbf{L} is not arbitrary as tabulated in Table 6.1. For those that satisfy the sampling criterion, we examine the support permissibility. In this singling out process, we found that only configuration A and B can possess edge-based permissibility if $LAT(\mathbf{L}^T)$ is quincunx. Configuration C is, however, either violating the sampling criterion or edge-based nonpermissible. Table 6.2 summarizes edge-based permissibility of the two-copy CMFB for each possible combination of $LAT(\mathbf{L}^T)$ and the three configurations. When the two-copy CMFB has edge-based permissibility (configuration A or B with quincunx $LAT(\mathbf{L}^T)$), cancellation of edge-based aliasing is possible. We have seen that edge-based aliasing can be completely cancelled if the prototype has linear phase as in (6.2) and the vector \mathbf{n}_s is as in (6.3).

It should be noted that even the best combinations of the configurations and $LAT(\mathbf{L}^T)$ can not achieve both edge-based and vertex-based permissibility. This imposes limitation on the attenuation of the individual filters in the two-copy CMFB as we will see in the design example.

6.4. Perfect Reconstruction Two-Copy CMFB

In this subsection, we present the perfect reconstruction conditions for edge-based permissible two-copy CMFB (configuration A or B with quincunx $LAT(\mathbf{L}^T)$). In the 1D case, the CMFB has perfect reconstruction if and only if the polyphase components of the prototype are pairwise power complementary [26]. We will see now the two-copy CMFB is paraunitary and hence has perfect reconstruction if and only if the polyphase components of the prototype satisfy some 2D power complementary conditions.

The analysis and synthesis filters. From the formulation of the analysis filters $H_m(\mathbf{w})$ in (6.1), the impulse response of $H_m(\mathbf{w})$ assumes the form

$$h_m(\mathbf{n}) = 2p(\mathbf{n}) \cos(2\pi(\mathbf{k}_m + \mathbf{b})^T \mathbf{N}^{-1} \mathbf{n}), \quad \mathbf{k} \in \mathcal{N}(\mathbf{N}^T), \quad m = 0, 1, \dots, J(\mathbf{M}) - 1, \quad (6.4)$$

where $\mathbf{b} = (0.5 \ 0)^T$ for configuration A and $\mathbf{b} = (0 \ 0.5)^T$ for configuration B . As the synthesis filter $F_m(\mathbf{w})$ is given by $F_m(\mathbf{w}) = H_m^*(\mathbf{w})$, the impulse responses of the analysis and synthesis filters are related by

$$f_m(\mathbf{n}) = h_m(-\mathbf{n}), \text{ where } \mathbf{n} \text{ is any } 2 \times 1 \text{ vector.}$$

Let the prototype have the following polyphase representation

$$P(\mathbf{w}) = \sum_{i=0}^{J(\mathbf{N})-1} E_i(\mathbf{N}^T \mathbf{w}) e^{-j\mathbf{w}^T \mathbf{n}_i}, \quad \mathbf{n}_i \in \mathcal{N}(\mathbf{N}), \quad (6.5)$$

$LAT(\mathbf{L}^T)$ configuration	lattice (a) (rectangular)	lattice (b) (rectangular)	lattice (c) (quincunx)
A		□	□ ■
B	□		□ ■
C	□	□	■

□ satisfied the sampling criterion
 ■ edge-based permissible

Table 6.2. The sampling criterion, edge-based permissibility and relation to three possible $LAT(\mathbf{L}^T)$ for configurations A, B and C. Lattice (a)–(c) in the table are as in Fig. 6.3 (a)–(c).

where $E_i(\mathbf{w})$ are the polyphase components of $P(\mathbf{z})$ and the vectors $\mathbf{n}_i \in \mathcal{N}(\mathbf{N})$ are ordered as in (3.2). Then the paraunitariness of the two-copy CMFB can be interpreted in terms of $E_i(\mathbf{w})$.

THEOREM 6.1 *Necessary and sufficient conditions for paraunitariness [31]. Consider the filter bank with decimation matrix \mathbf{M} in Fig. 1.1. Let the matrix \mathbf{N} be given by $\mathbf{N} = \mathbf{M}\mathbf{L}$, where $LAT(\mathbf{L}^T)$ is quincunx. Choose the analysis filters $H_m(\mathbf{w})$ as in (6.4) and let the synthesis filters $F_m(\mathbf{w}) = H_m^*(\mathbf{w})$. Also let the prototype be linear phase with $p(\mathbf{n}) = p(\mathbf{n}_s - \mathbf{n})$ and $\mathbf{n}_s = \mathbf{N}(0.5 \ 0.5)^T \bmod \mathbf{N}$. Then the two-copy CMFB is paraunitary (i.e., the polyphase matrix is paraunitary) if and only if*

$$E_i^*(\mathbf{w})E_i(\mathbf{w}) + E_{i+J(\mathbf{M})}^*(\mathbf{w})E_{i+J(\mathbf{M})}(\mathbf{w}) = c, \quad (6.6)$$

where c is some constant.

Remark on Theorem 6.1. The condition in (6.6) is equivalent to saying that $E_i(\mathbf{w})$ and $E_{i+J(\mathbf{M})}(\mathbf{w})$ are power complementary in 2D sense. This condition can be satisfied by using the 2D paraunitary lattice, [34]. Also the theorem holds for both configuration A and B.

Properties of the two-copy CMFB

1. *The analysis and synthesis filters.* In a 1D CMFB, each analysis filter has two distinct shifts of the prototype filter. So the total bandwidth of each individual filter is the same.

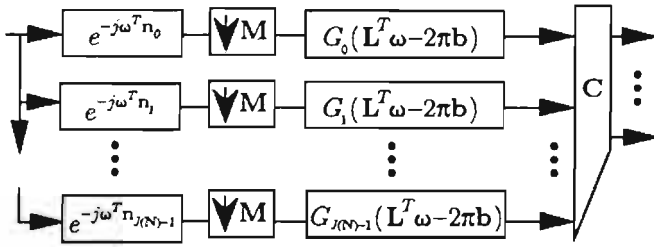


Figure 6.8. Efficient implementation of the analysis bank of the two-copy cosine modulated filter bank. The matrix \mathbf{C} is of dimension $|\det \mathbf{M}|$ by $2|\det \mathbf{M}|$.

For 2D filters, total bandwidth should be interpreted as the total spectral occupancy. It can be shown that due to quincunx $LAT(L^T)$, each analysis filters in the two-copy CMFB consists of two distinct shifts of the prototype and has the same size of spectral occupancy.

2. *Polyphase components of the prototype.* In the 1D CMFB, the polyphase components of the prototype are related in pairs because of linear phase constraint of the prototype. At the same time, there are also power complementary pairs due to paraunitariness. Furthermore if half of the polyphase components are pairwise power complementary, the other half, due to linear phase, are automatically pairwise power complementary, as shown in [26]. The situation is exactly the same in the two-copy CMFB [31].
3. *Efficient implementation of the two-copy CMFB.* Efficient implementation is one of the reasons that cosine modulated filter banks attract a lot of attention. In the 1D CMFB, the complexity of the analysis bank or the synthesis bank is that of the prototype filter plus a DCT matrix. The DCT matrices are known to be low-complexity matrices [56]. There also exists efficient implementation for the two-copy CMFB. The cost of the analysis bank or the synthesis bank is that of a prototype filter plus a matrix, which has elements resembling that of a nonseparable 2D DCT matrix. To be more specific, by using the polyphase representation of the prototype in (6.5), the analysis filters in (6.4) can be rewritten as

$$H_m(\mathbf{w}) = \sum_{i=0}^{J(\mathbf{N})-1} 2E_i(\mathbf{N}^T \mathbf{w} - 2\pi \mathbf{b})[\mathbf{C}]_{mi} \exp(-j\mathbf{w}^T \mathbf{n}_i),$$

$$m = 0, 1, \dots, J(\mathbf{M}) - 1,$$

where

$$[\mathbf{C}]_{mi} = \cos(2\pi(\mathbf{k}_m + \mathbf{b})^T \mathbf{N}^{-1} \mathbf{n}_i),$$

$$m = 0, 1, \dots, J(\mathbf{M}) - 1, \quad i = 0, 1, \dots, J(\mathbf{N}) - 1.$$

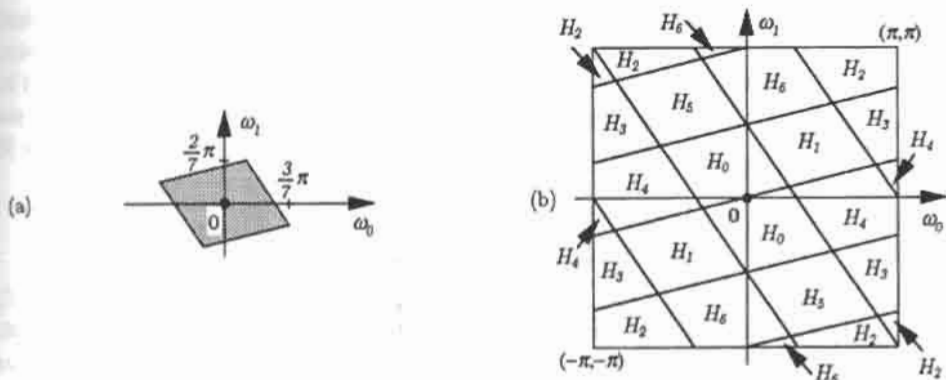


Figure 6.9. Example 6.1. Two-copy cosine modulated filter bank. (a) Spectral support of the prototype $P(w)$, $SPD(\pi N^{-T})$, and (b) supports of the analysis filters.

The above expression for the analysis filters gives rise to the efficient implementation in Fig. 6.8. The matrix C is rectangular of dimension $J(M) \times J(N)$. The figure demonstrates that the complexity of the 2D CMFB is that of the prototype plus C , which can be decomposed into 1D DCT matrices of smaller dimensions.

Example 6.1. Two-copy CMFB. Let $M = \begin{pmatrix} 7 & -2 \\ 0 & 1 \end{pmatrix}$. Choose $L = \begin{pmatrix} 1 & 1 \\ 2 & 4 \end{pmatrix}$, then

$LAT(L^T)$ is quincunx. The matrix N given by $N = ML$ is $N = \begin{pmatrix} 3 & -1 \\ 2 & 4 \end{pmatrix}$. Fig. 6.9(a)

shows the support of the prototype. If we choose configuration B , the supports of the analysis filters are as shown in Fig. 6.9(b). By Theorem 6.1, the two-copy CMFB has perfect reconstruction if the polyphase components of the prototype satisfy the power complementary condition given in (6.6). Fig. 6.10 shows the support of impulse response of the prototype filter, $p(n_0, n_1)$. The support of $p(n_0, n_1)$ resembles the shape of $SPD(2N)$. Each solid dot represents a possibly nonzero coefficient of $p(n_0, n_1)$. In this optimization, each of the fourteen polyphase components has four coefficients. The corresponding frequency response of the prototype is shown in Fig. 6.11. The stopband attenuation of the prototype is 17 dB. Since vertex-based permissibility is not achievable in any of our construction, the attenuation of the prototype can not be arbitrary good like in 1D case.

6.5. Further Discussion on the Construction of the Two-Copy CMFB

In this subsection, we would like to go back to the construction process of two-copy CMFB and have a more detailed discussion of some of the subjects that require a more careful examination.

Support of the prototype. The support of the prototype filter is $SPD(\pi N^{-T})$. The spectral supports of the individual filters depend on the choice of configurations and the

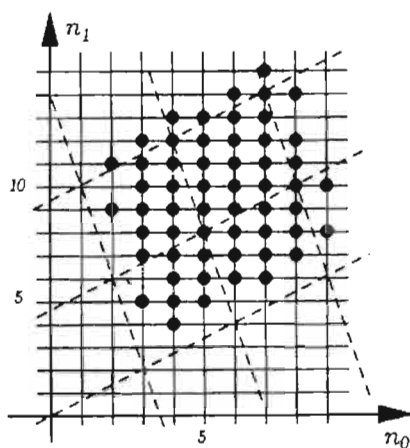


Figure 6.10. Example 6.1. Two-copy cosine modulated filter bank. The impulse response support of the prototype. Each solid dot represents a possibly non-zero coefficient of the prototype. (Intersection points of the dashed lines are on the lattice of \mathbf{N} . Solid lines represent integers.)

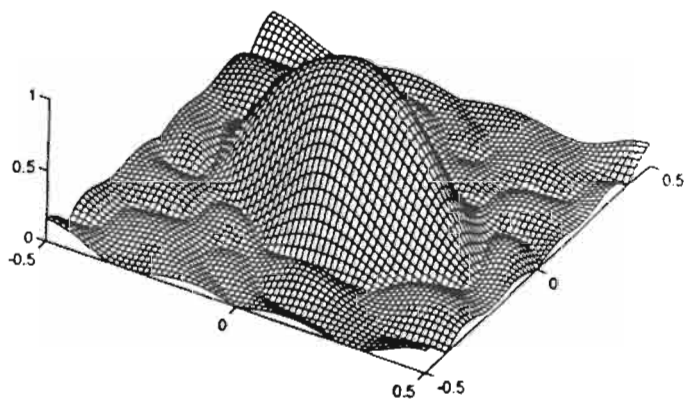


Figure 6.11. Example 6.1. Two-copy cosine modulated filter bank. The magnitude response of the prototype with frequency normalized by 2π .

matrix $\mathbf{N} = \mathbf{M}\mathbf{L}$. Although the decimation matrix \mathbf{M} is arbitrary, \mathbf{L} is subject to the constraint that $LAT(\mathbf{L}^T)$ is quincunx. The matrix \mathbf{N} is not arbitrary and hence the support of the prototype is not arbitrary. In the construction of the two-copy CMFB, for a given \mathbf{M} we formulate $\mathbf{N} = \mathbf{M}\mathbf{L}$ for some integer matrix \mathbf{L} with quincunx $LAT(\mathbf{L}^T)$. It follows that \mathbf{N} assumes the form

$$\mathbf{N} = \mathbf{M}' \begin{pmatrix} 1 & 1 \\ -1 & 1 \end{pmatrix}, \quad \text{for some integer matrix } \mathbf{M}'. \quad (6.7)$$

Conversely, it can be shown for any \mathbf{N} of the form in (6.7), we can construct a $J(\mathbf{M}')$ channel two-copy CMFB with decimation matrix \mathbf{M}' such that the prototype filter has support $SPD(\pi\mathbf{N}^{-T})$. However, we should be careful with this statement. Consider

$$\mathbf{N} = \begin{pmatrix} 4 & 0 \\ 4 & 2 \end{pmatrix},$$

which takes the form

$$\mathbf{N} = \underbrace{\begin{pmatrix} 2 & -2 \\ 3 & -1 \end{pmatrix}}_{\mathbf{M}_1} \underbrace{\begin{pmatrix} 1 & 1 \\ -1 & 1 \end{pmatrix}}_{\mathbf{L}_1} \quad \text{or the form} \quad \mathbf{N} = \underbrace{\begin{pmatrix} 4 & 0 \\ 4 & 1 \end{pmatrix}}_{\mathbf{M}_2} \underbrace{\begin{pmatrix} 1 & 0 \\ 0 & 2 \end{pmatrix}}_{\mathbf{L}_2}.$$

Using $SPD(\pi\mathbf{N}^{-T})$ as the prototype support, the 4-channel filter bank with decimation matrix \mathbf{M}_1 has edge-based permissibility while the 4-channel filter bank with decimation matrix \mathbf{M}_2 does not have edge-based permissibility.

Remark on the choice $\mathbf{N}=\mathbf{M}\mathbf{L}$. In Sec. 6.2., we have seen that when the prototype $P(\mathbf{w})$ is decimated and then expanded by \mathbf{M} , the images are confined to the grid formed by the filters in the DFT filter bank. Furthermore, $P(\mathbf{w})$ and its image form a pattern resembling that of $LAT(\mathbf{L}^T)$. This is a direct result of the choice $\mathbf{N} = \mathbf{M}\mathbf{L}$ [31]. If we had chosen $\mathbf{N} = \mathbf{L}\mathbf{M}$, then in general the images of $P(\mathbf{w})$ would not be confined to the grid formed by shifts of $P(\mathbf{w})$ in the DFT filter bank.

More general \mathbf{L} ? In the preceding construction of two-copy CMFB, we have assumed \mathbf{L} to be an integer matrix of determinant 2. There are only three possible $LAT(\mathbf{L}^T)$. Consider the k th subband in configuration A . From the discussion in Sec. 6.3, we know that $Q_{A,k}(\mathbf{w})$ is always edge-adjacent to its own images for rectangular $LAT(\mathbf{L}^T)$ and $Q_{A,k}(\mathbf{w})$ is always vertex-adjacent to its own images for quincunx $LAT(\mathbf{L}^T)$. In this case the best solution of two-copy CMFB available to us is edge-based permissible but not vertex-based permissible. One wonders whether it is possible to derive a solution of two-copy CMFB that is both edge-based permissible and vertex-based permissible if \mathbf{L} is not restricted to be an integer matrix. The answer is still unfortunately, no! When \mathbf{L} is not an integer matrix but has determinant 2, it can be shown that in some special cases $Q_{A,k}(\mathbf{w})$ is neither edge-adjacent nor vertex-adjacent to any of its own images. In this case, however, the images of passbands of $Q_{A,k}(\mathbf{w})$ will always overlap with passbands of $Q'_{A,k}(\mathbf{w})$; the sampling criterion is violated. The filter bank can not have perfect reconstruction even if all the filters are ideal. This discussion also holds for configuration B and C .

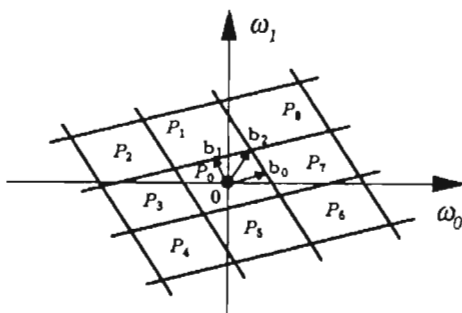


Figure 7.1. DFT filter bank example.

7. Four-Copy Cosine Modulated Filter Banks

In the two-copy CMFB, each analysis filter consists of two copies of the prototype, while in the four-copy CMFB, each analysis filter consists of four copies of the prototype. The general setting of the four-copy CMFB will be an analogy of two-copy CMFB. But some procedures used in the two-copy CMFB require some modifications for the four-copy case (Sec. 7.1). In the two-copy CMFB, we have found that it is not possible to have both edge-based and vertex-based permissibility. In the four-copy case, it is possible but the four-copy CMFB can be edge-based and vertex-based permissible (i.e., completely permissible) only with one particular configuration. This special case of completely permissible four-copy CMFB will be discussed in Sec. 7.2. All the other possible cases of four-copy CMFB will be discussed in Sec. 7.3.

7.1. General Setting

For a four-copy CMFB with decimation matrix \mathbf{M} and $J(\mathbf{M})$ channels, we start from a DFT filter bank with four times the number of channels. Then we shift the filters in the DFT filter bank and combine four shifted filters to obtain real-coefficient analysis filters. However, the procedure of combining four filters to obtain real-coefficient analysis filters is not as straightforward as in the two-copy case.

Similar to the two-copy case, given decimation matrix \mathbf{M} , we start from a DFT filter bank with decimation matrix $\mathbf{N} = \mathbf{M}\mathbf{L}$, where \mathbf{L} is an integer matrix with $|\det \mathbf{L}| = 4$. Suppose the $4J(\mathbf{M})$ -channel DFT filter bank has supports as shown in Fig. 7.1. We can shift the filters in the three directions (\mathbf{b}_0 , \mathbf{b}_1 , and \mathbf{b}_2) indicated in Fig. 7.1. Fig. 7.2 shows the shifted filters with respect to the three shifts. For instance, if we shift the filters by \mathbf{b}_2 , the resulting supports are as shown in Fig. 7.2(c). The shifted filters are denoted by $Q_{C,i}$ and $Q'_{C,i}$. Notice that the impulse response of $Q_{C,i}$ and $Q'_{C,i}$ are conjugates of each other. Later when we derive the real-coefficient analysis filters, $Q_{C,i}$ and $Q'_{C,i}$ should always belong to the same analysis filter. The set $(Q_{C,i}, Q'_{C,i})$ will be called a conjugate pair. There is a total of

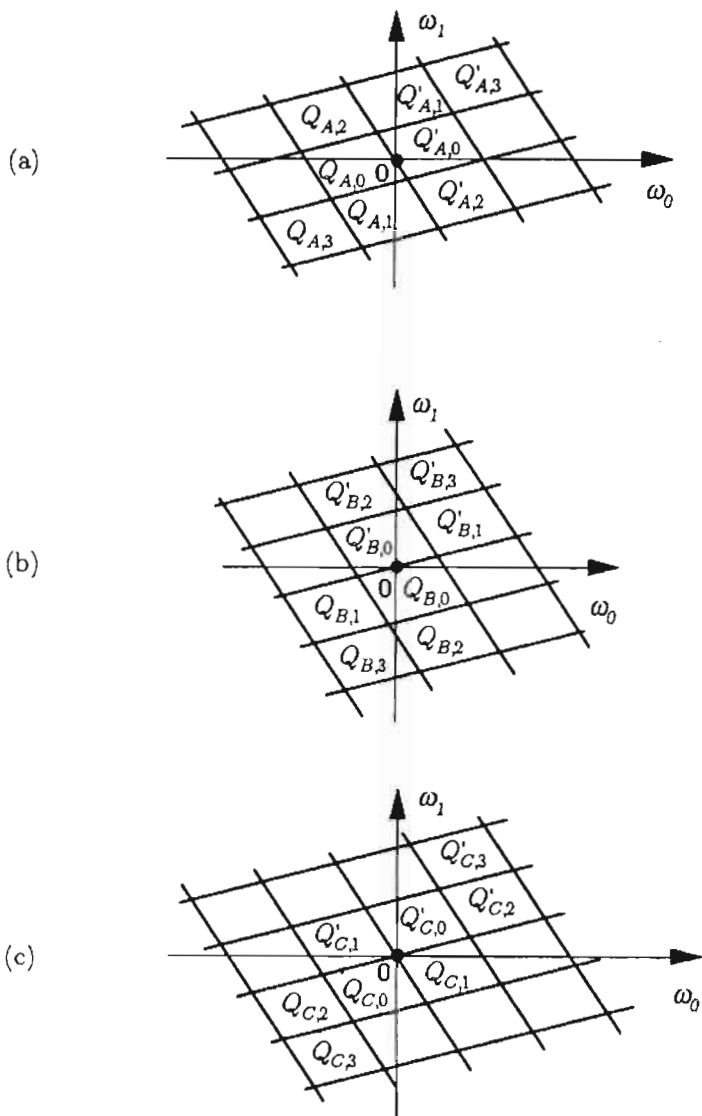


Figure 7.2. Shifted versions of the filters in the DFT filter bank.

$2J(\mathbf{M})$ conjugate pairs. Similarly, in Fig. 7.2(a) and Fig. 7.2(b) $(Q_{A,i}, Q'_{A,i})$ is a conjugate pair and $(Q_{B,i}, Q'_{B,i})$ is a conjugate pair. As each analysis filter in the four-copy CMFB has four copies of the prototype, each analysis filter consists of two conjugate pairs.

The procedure of combining four shifted filters

Recall that in the two-copy CMFB, after we shift the filters in one of the three directions, there is a unique way to pair the filters and obtain real-coefficient analysis filters. However, in the four-copy CMFB, we have a number of ways to combine the filters. Consider the lowpass analysis filter $H_0(\mathbf{w})$ only. In Fig. 7.2(c), if we combine the pair $(Q_{C,0}, Q'_{C,0})$ and the pair $(Q_{C,1}, Q'_{C,1})$, then the support of $H_0(\mathbf{w})$ is as shown in Fig. 7.3(a). If we combine $(Q_{C,0}, Q'_{C,0})$ and $(Q_{C,2}, Q'_{C,2})$, then the support of $H_0(\mathbf{w})$ is as shown in Fig. 7.3(b). Another possible choice is to have $H_0(\mathbf{w})$ as in Fig. 7.3(c) by combining $(Q_{C,0}, Q'_{C,0})$ and $(Q_{C,3}, Q'_{C,3})$. Notice that in all three choices of $H_0(\mathbf{w})$, the support of $H_0(\mathbf{w})$ is connected by edge or vertex. So even with the constraint that the support of $H_0(\mathbf{w})$ should be a connected region, the support of $H_0(\mathbf{w})$ cannot be uniquely determined. Therefore, it is possible to derive several different configurations from Fig. 7.2. But of all the configurations derived from Fig. 7.2(a)–(c), only one configuration can lead to edge-based and vertex-based permissible four-copy CMFB, which is discussed next.

7.2. The Simplistic Four-Copy CMFB

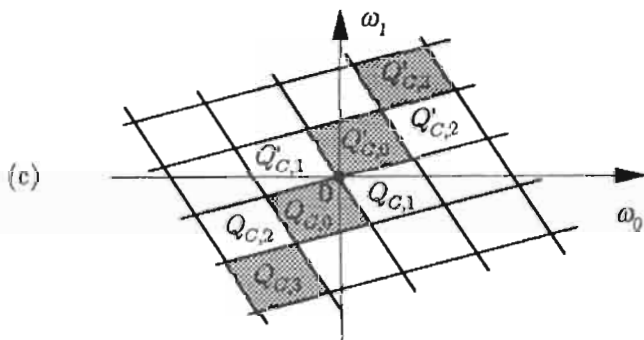
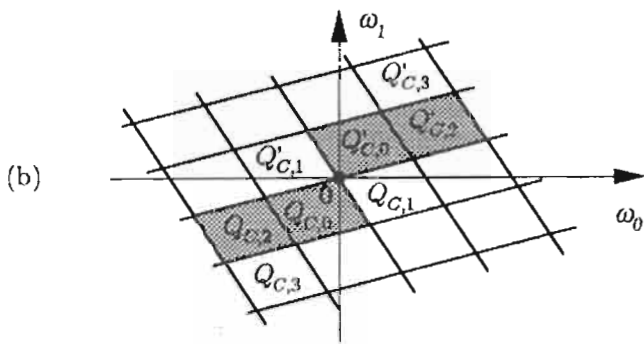
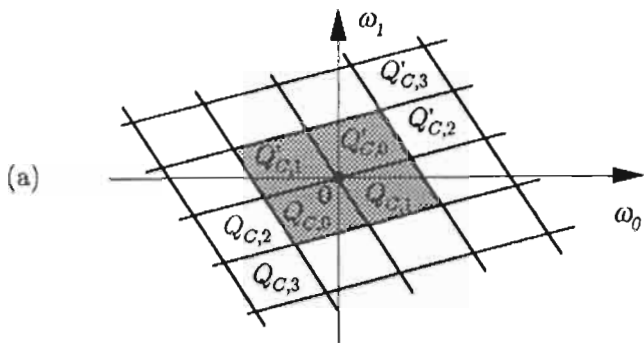
We consider a special type of four-copy CMFB, which will be called the simplistic four-copy CMFB. In the simplistic four-copy CMFB,

$$\mathbf{L} = \begin{pmatrix} 2 & 0 \\ 0 & 2 \end{pmatrix}$$

and the lowpass analysis filter $H_0(\mathbf{w})$ is chosen as in Fig. 7.3(a). So the lowpass analysis filter has a parallelogram support $SPD(\pi\mathbf{M}^{-T})$, which is a natural generalization of the lowpass analysis filter of a separable CMFB. In this case, it can be shown that if the four-copy CMFB has both edge-based and vertex-based permissibility then the decimation matrix \mathbf{M} is restricted to one of the following forms.

$$\mathbf{M} = \mathbf{U}\mathbf{A}_1, \quad (\text{case 1}) \quad \text{and} \quad \mathbf{M} = \mathbf{K}\mathbf{A}_2, \quad (\text{case 2}) \quad (7.1)$$

where \mathbf{U} is unimodular, \mathbf{K} has $|\det \mathbf{K}| = 2$ and \mathbf{A}_1 and \mathbf{A}_2 are diagonal. All matrices are integer matrices. For the first case of \mathbf{M} , the support configurations of the analysis and synthesis filters can be obtained by designing two 1D perfect reconstruction filter banks and performing a unimodular transformation as explained in Sec. III [49]. If the two 1D filter banks are cosine modulated, then the resulting 2D nonseparable filter bank will also be cosine modulated. That is, all the filters in the 2D nonseparable filter bank can be derived from one prototype. For the second case, the desired support configuration of four-copy CMFB can be achieved by concatenating a separable 2D CMFB with a 2D nonseparable



■ support of $H_0(\omega)$

Figure 7.3. Possible supports of $H_0(\omega)$ when different conjugate pairs are chosen.

two-channel filter bank in the form of a tree structure. We have seen such a tree structure in Example 4.3. In this case, even if the two systems are cosine modulated, the cascaded system is not cosine modulated in general. But the 2D filter banks designed in this method have the desired support configuration of a four-copy CMFB and have perfect reconstruction.

7.3. Other Possible Forms of Four-Copy CMFB

For the most general four-copy CMFB, the only requirement is that each filter contains four copies of the prototype. The support of the lowpass analysis filter is not necessarily a parallelogram as we have seen in Sec. 7.1. The matrix \mathbf{L} can be any integer matrix with $|\det \mathbf{L}| = 4$. Similar to the two-copy CMFB, the locations of images of analysis filters are determined by $LAT(\mathbf{L}^T)$. With $|\det \mathbf{L}^T| = 4$, there are 7 possible choices for $LAT(\mathbf{L}^T)$. Consider the lowpass analysis filter that has spectral support consisting of four connected parallelograms. Namely, any one of the four parallelograms is edge-adjacent or vertex-adjacent to another parallelogram. In this case, it can be verified that such a filter bank can not possess both edge-based permissibility and vertex-based permissibility for any choice of $LAT(\mathbf{L}^T)$, except in some special degenerate cases.

Remarks on four-copy CMFB. We must note that the discussion of alias cancellation is made completely from the viewpoint of support permissibility. Although in the discussion, the analysis filters are described as cosine modulated versions of a prototype filter, the argument continues to hold even if the filter bank is not cosine modulated. In all the discussion, the assumptions actually made are (1) the analysis and synthesis filters have the same spectral support, which is in general true in most filter banks, and (2) the lowpass analysis filter consist of four connected parallelograms. With these two assumptions, we can make the following conclusion. Consider a 2D filter bank, in which the analysis filters contain four parallelograms. Suppose the four parallelograms of the lowpass analysis are connected. If such a filter bank can possess both edge-based permissibility and vertex-based permissibility, then \mathbf{M} is either as given in (7.1) or limited to some degenerate cases.

8. Two-Dimensional FIR Lossless Matrices

A large subclass of filter banks is the so-called orthonormal filter banks. In these systems, the polyphase matrix of the analysis bank $\mathbf{E}(z)$ is paraunitary, i.e., $\tilde{\mathbf{E}}(z)\mathbf{E}(z) = \mathbf{I}_M$. [50]. Characterization of such matrices is therefore useful. For 1D systems, this has already been done and the results are well known. In this section, we will consider the 2D counterpart of this topic. Recall from Sec. 1.2 that a causal, stable paraunitary system is also termed as a lossless system.

Characterization of 2D FIR lossless systems. Similar to the 1D case, 2D causal systems can be described by state space description. Several state space realizations have been proposed for 2D causal systems. For the characterization of the 2D lossless systems, the first-level realization [16], [57] and the Roesser realization [40] are of particular importance. The 2D FIR lossless systems have been successfully characterized in terms of first-level

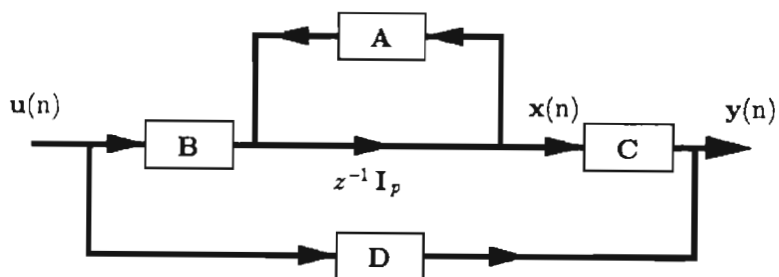


Figure 8.1. The schematic of the state space description for $E(z)$.

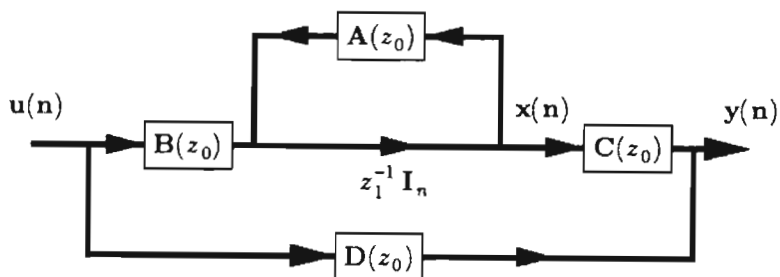


Figure 8.2. The schematic of the first-level description for $E(z)$.

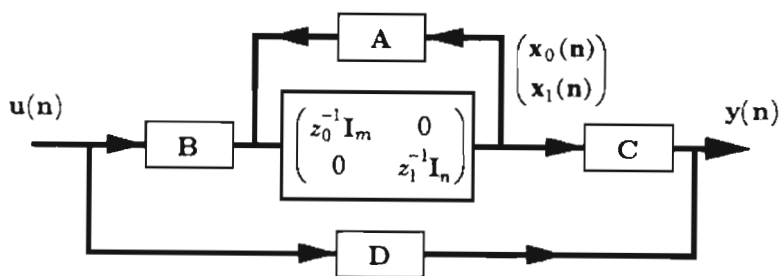


Figure 8.3. The schematic of the Roesser state space description for $E(z)$.

realization [4], [51] and Roesser realization [51]. Losslessness of a 2D system is directly related to the realization matrices in these two types of state space description.

Factorization of 2D FIR lossless systems. Recall in 1D case, any lossless systems can be factorized into degree-one building blocks. To address the issue of factorizing 2D lossless systems, we need to define the degree of a 2D causal transfer matrix first. Consider a 2D causal system $\mathbf{E}(\mathbf{z})$, where $\mathbf{z} = (z_0 \ z_1)^T$. If we hold z_0 fixed, we can view $\mathbf{E}(\mathbf{z})$ as a 1D system in z_1 and in this case we can define the degree of $\mathbf{E}(\mathbf{z})$ in z_1 as in 1D case. The degree of $\mathbf{E}(\mathbf{z})$ in z_0 can be defined in a similar manner. As in 1D case, we are interested in factorizing a FIR lossless system $\mathbf{E}(\mathbf{z})$ into systems of lower degree in z_0, z_1 or in both variables. It can be shown that the factorizability of a 2D FIR lossless system $\mathbf{E}(\mathbf{z})$ can be translated into properties of first-level realization and Roesser realization [51]. We will also present a subclass of 2D FIR lossless systems that can be expressed as a product of 1D FIR lossless systems [34].

The main purpose of this section is to review some important developments of 2D FIR lossless systems. A brief review of 1D lossless systems is given in Sec. 8.1. Results on 1D lossless systems will be mentioned only when a related 2D result is to be discussed in this paper. For a more thorough treatment of 1D lossless system, the readers can refer to Chapter 14, [50]. In Sec. 8.2, we introduce the first-level realization [16], [57] and the Roesser realization [40]. Then we characterize the 2D FIR lossless systems through these two realizations. Results on factorization of 2D FIR lossless systems [34], [23], [51], are presented in Sec. 8.3.

8.1. One-Dimensional FIR Lossless Matrices

State space description

Let $\mathbf{E}(z)$ be a 1D $M \times M$ causal rational system that can be implemented with p delay elements. Denote the output of the i th delay element by $x_i(n)$ and let

$$\mathbf{x}(n) = (x_0(n) \ x_1(n) \ \dots \ x_{p-1}(n))^T.$$

Then the input $\mathbf{u}(n)$ and output $\mathbf{y}(n)$ of $\mathbf{E}(z)$ can be related by the following description.

$$\begin{aligned} \mathbf{x}(n+1) &= \mathbf{A}\mathbf{x}(n) + \mathbf{B}\mathbf{u}(n) \\ \mathbf{y}(n) &= \mathbf{C}\mathbf{x}(n) + \mathbf{D}\mathbf{u}(n) \end{aligned} \quad (8.1)$$

The quadruple $(\mathbf{A}, \mathbf{B}, \mathbf{C}, \mathbf{D})$ is called the state space description of $\mathbf{E}(z)$ and the matrix

$$\mathbf{R} = \begin{pmatrix} \mathbf{A} & \mathbf{B} \\ \mathbf{C} & \mathbf{D} \end{pmatrix}$$

is called the realization matrix. It can be shown that any causal rational system $\mathbf{E}(z)$ has a state space description as in (8.1). Also from (8.1), we can write $\mathbf{E}(z)$ as

$$\mathbf{E}(z) = \mathbf{C}(z\mathbf{I} - \mathbf{A})^{-1}\mathbf{B} + \mathbf{D},$$

where \mathbf{A} is of dimension $p \times p$. When p is equal to the degree of $\mathbf{E}(z)$, we say the state space realization is minimal. Fig. 8.1 shows the schematic of the state space description.

In the theorem below, we will see that FIR lossless systems can be characterized in terms of their realization matrices [50].

THEOREM 8.1 *FIR lossless systems and state space realization [46], [14]. A system $\mathbf{E}(z)$ is FIR lossless if and only if $\mathbf{E}(z)$ admits a minimal realization such that the realization matrix \mathbf{R} is unitary, i.e. $\mathbf{R}^T \mathbf{R} = \mathbf{I}$, and \mathbf{A} is strictly lower triangular. Moreover, the degree of a lossless system $\mathbf{E}(z)$ is equal to the degree of $[\det \mathbf{E}(z)]$.*

THEOREM 8.2 *Factorization of FIR lossless matrices [50]. An $M \times M$ FIR lossless system $\mathbf{E}(z)$ with degree ρ can always be factorized as*

$$\mathbf{E}(z) = \mathbf{V}_\rho(z) \mathbf{V}_{\rho-1}(z) \dots \mathbf{V}_1(z) \mathbf{E}_0, \quad (8.2)$$

where \mathbf{E}_0 is a $M \times M$ unitary matrix and $\mathbf{V}_n(z)$ is an $M \times M$ FIR lossless matrix of degree one given by

$$\mathbf{V}_n(z) = \mathbf{I} - \mathbf{v}_n \mathbf{v}_n^T + z^{-1} \mathbf{v}_n \mathbf{v}_n^T, \quad \text{with } \mathbf{v}_n^T \mathbf{v}_n = 1. \quad (8.3)$$

8.2. Two-dimensional FIR lossless matrices

8.2.1. First-Level Realization

Let $\mathbf{E}(z)$ be a 2D causal rational system. If we hold z_0 fixed, we can view it as 1D system in z_1 , with the coefficients dependent on z_0 . Consider a 1D realization of this system and let the state space realization be $(\hat{\mathbf{A}}(z_0), \hat{\mathbf{B}}(z_0), \hat{\mathbf{C}}(z_0), \hat{\mathbf{D}}(z_0))$. Then the system can be expressed as

$$\mathbf{E}(z) = \hat{\mathbf{D}}(z_0) + \hat{\mathbf{C}}(z_0)(z_1 \mathbf{I}_n - \hat{\mathbf{A}}(z_0))^{-1} \hat{\mathbf{B}}(z_0). \quad (8.4)$$

This is termed the first-level realization of $\mathbf{E}(z)$. Notice that $\hat{\mathbf{A}}(z_0)$ is an $n \times n$ matrix function of z_0 . The matrix

$$\mathbf{F}(z_0) = \begin{pmatrix} \hat{\mathbf{A}}(z_0) & \hat{\mathbf{B}}(z_0) \\ \hat{\mathbf{C}}(z_0) & \hat{\mathbf{D}}(z_0) \end{pmatrix}$$

is termed the system matrix associated with this realization. The realization is called minimal if $n = \mu$, where μ is the degree of $\mathbf{E}(z)$ in z_1 . The following result is shown in [4], [51].

THEOREM 8.3 *2D FIR lossless systems and first-level realization. The system $\mathbf{E}(z)$ with degree ρ in z_0 and μ in z_1 is FIR lossless if and only if there exists a minimal first-level realization such that the system matrix $\mathbf{F}(z_0)$ is FIR lossless and all the eigenvalues of $\hat{\mathbf{A}}(z_0)$ are 0 for all z_0 . In this case, $\mathbf{F}(z_0)$ has degree ρ .*

8.2.2. Roesser Realization

Roesser proposed the following state space description for 2D causal rational $\mathbf{E}(z)$ [5], [40].

$$\begin{pmatrix} \mathbf{x}_0(n_0 + 1, n_1) \\ \mathbf{x}_1(n_0, n_1 + 1) \end{pmatrix} = \mathbf{A} \begin{pmatrix} \mathbf{x}_0(n_0, n_1) \\ \mathbf{x}_1(n_0, n_1) \end{pmatrix} + \mathbf{B}\mathbf{u}(n_0, n_1),$$

$$\mathbf{y}(n_0, n_1) = \mathbf{C} \begin{pmatrix} \mathbf{x}_0(n_0, n_1) \\ \mathbf{x}_1(n_0, n_1) \end{pmatrix} + \mathbf{D}\mathbf{u}(n_0, n_1).$$

So $\mathbf{E}(z)$ can be expressed as

$$\mathbf{E}(z) = \mathbf{D} + \mathbf{C} \left(\begin{pmatrix} z_0 \mathbf{I}_m & \mathbf{Q} \\ \mathbf{Q} & z_1 \mathbf{I}_n \end{pmatrix} - \mathbf{A} \right)^{-1} \mathbf{B}. \quad (8.5)$$

Similar to 1D case, the realization matrix \mathbf{R} is defined as

$$\mathbf{R} = \begin{pmatrix} \mathbf{A} & \mathbf{B} \\ \mathbf{C} & \mathbf{D} \end{pmatrix}.$$

Let $\mathbf{E}(z)$ be of degree ρ in z_0 and μ in z_1 . The realization is minimal if $m = \rho$ and $n = \mu$. A schematic of the Roesser realization is shown in Fig. 8.2.

Before we characterize the 2D FIR lossless matrices in terms of the Roesser realization, the definition of the 2D characteristic polynomial is in order. The 2D characteristic polynomial of a $p \times p$ matrix \mathbf{Q} with partition $(m, p - m)$ is

$$\alpha_{m, p-m}(z_0, z_1) = \det \left[\begin{pmatrix} z_0 \mathbf{I}_m & \mathbf{Q} \\ \mathbf{Q} & z_1 \mathbf{I}_{p-m} \end{pmatrix} - \mathbf{Q} \right]. \quad (8.6)$$

THEOREM 8.4 [51] *A causal 2D transfer matrix $\mathbf{E}(z)$ is FIR lossless if and only if there exists a minimal Roesser realization such that the realization matrix \mathbf{R} is unitary and the 2D characteristic polynomial of \mathbf{A} satisfies $\alpha_{\rho, \mu}(z_0, z_1) = z_0^\rho z_1^\mu$. Moreover, if $\mathbf{E}(z)$ is FIR lossless with degree ρ in z_0 and μ in z_1 , then $\det \mathbf{E}(z) = cz_0^{-\rho} z_1^{-\mu}$, with $|c| = 1$.*

8.3. Factorization of 2D FIR Lossless Systems

In this subsection, we present some results on the factorization of 2D FIR lossless matrices. We will see that a 2D causal FIR system $\mathbf{E}(z)$ can be factorized into FIR lossless systems of lower degree in z_1 if the first-level system matrix is of a certain form (Theorem 8.5). Similarly, we will see that a 2D causal system $\mathbf{E}(z)$ can be factorized into FIR lossless systems of lower degree in z_0 and z_1 if the Roesser realization matrix is of a certain form (Theorem 8.6). These two theorems are proved in [51]. Finally, in Theorem 8.7 we will introduce a subclass of 2D FIR lossless systems that can be factorized into the 1D building blocks in (8.3). This subclass consists of 2D FIR lossless systems that have order one in z_0 or z_1 [34].

Before we present the theorems, we look at a structure that leads to 2D FIR lossless systems. A generalization of the factorization in (8.2) to 2D case is [23], [51]

$$\mathbf{E}(\mathbf{z}) = \mathbf{U}_\rho(\mathbf{z})\mathbf{U}_{\rho-1}(\mathbf{z}) \dots \mathbf{U}_1(\mathbf{z})\mathbf{E}_0, \quad (8.7)$$

where \mathbf{E}_0 is unitary, and $\mathbf{U}_n(\mathbf{z})$ is a 1D degree-one building block of the form $\mathbf{V}_n(z_0)$ or $\mathbf{V}_n(z_1)$ as defined in (8.3). The systems constructed in this manner are FIR and lossless. However, they only represent a subclass of 2D FIR lossless systems. The reason will follow from Theorem 8.6 below.

THEOREM 8.5 [51] *A 2D FIR lossless system $\mathbf{E}(\mathbf{z})$ with degree μ in z_1 can be factorized as $\mathbf{E}(\mathbf{z}) = \mathbf{E}_1(\mathbf{z})\mathbf{E}_2(\mathbf{z})$, where $\mathbf{E}_i(\mathbf{z})$ are of degree μ_i in z_1 and $\mu = \mu_1 + \mu_2$, if and only if $\mathbf{E}(\mathbf{z})$ admits a minimal first-level realization such that all the following conditions are satisfied.*

1. The system matrix $\mathbf{F}(z_0)$ is FIR and lossless in z_0 .
2. The matrix $\widehat{\mathbf{A}}(z_0)$ in (8.4) is block lower triangular, i.e.

$$\widehat{\mathbf{A}}(z_0) = \begin{pmatrix} \widehat{\mathbf{A}}_1(z_0) & \mathbf{Q} \\ \times & \widehat{\mathbf{A}}_2(z_0) \end{pmatrix}, \quad (8.8)$$

where \times represent possibly nonzero polynomial in z_0^{-1} .

3. The block matrix $\widehat{\mathbf{A}}_i(z_0)$ is of dimension $\mu_i \times \mu_i$ and all the eigenvalues of $\widehat{\mathbf{A}}_i(z_0)$ are 0 for all z_0 .

A corollary of this theorem is that FIR lossless $\mathbf{E}(\mathbf{z})$ can be factorized into matrices of degree-one in z_1 if and only if $\widehat{\mathbf{A}}(z_0)$ is strictly lower triangular.

THEOREM 8.6 [51] *Let $\mathbf{E}(\mathbf{z})$ be a 2D FIR lossless system with degree ρ in z_0 and μ in z_1 . It can be factorized as $\mathbf{E}(\mathbf{z}) = \mathbf{E}_1(\mathbf{z})\mathbf{E}_2(\mathbf{z})$, where $\mathbf{E}_i(\mathbf{z})$ are of degree ρ_i in z_0 and μ_i in z_1 with $\rho = \rho_1 + \rho_2$ and $\mu = \mu_1 + \mu_2$, if and only if the following holds: $\mathbf{E}(\mathbf{z})$ should admit a minimal Roesser realization $(\mathbf{A}, \mathbf{B}, \mathbf{C}, \mathbf{D})$ such that all the following conditions are satisfied.*

1. The realization matrix \mathbf{R} is unitary.
2. The matrix \mathbf{A} in (8.5) is of the form

$$\mathbf{A} = \begin{pmatrix} \mathbf{A}_{11} & \mathbf{Q} & \mathbf{A}_{12} & \mathbf{Q} \\ \times & \mathbf{A}_{21} & \times & \mathbf{A}_{22} \\ \mathbf{A}_{13} & \mathbf{Q} & \mathbf{A}_{14} & \mathbf{Q} \\ \times & \mathbf{A}_{23} & \times & \mathbf{A}_{24} \end{pmatrix},$$

where \times represent possibly nonzero entry.

3. The matrix $\mathbf{A}_i = \begin{pmatrix} \mathbf{A}_{i1} & \mathbf{A}_{i2} \\ \mathbf{A}_{i3} & \mathbf{A}_{i4} \end{pmatrix}$ with partition (ρ_i, μ_i) has characteristic polynomial $\alpha_{\rho_i, \mu_i}(\mathbf{z}) = z_0^{\rho_i} z_1^{\mu_i}$.

A corollary of this theorem is that FIR lossless $\mathbf{E}(\mathbf{z})$ can be factorized into 1D degree-one building block as in (8.7) if and only if \mathbf{A} is of the form $\mathbf{A} = \mathbf{P}^T \mathbf{L} \mathbf{P}$, where \mathbf{P} is a permutation matrix and \mathbf{L} is strictly lower triangular.

THEOREM 8.7 [34] *Let $\mathbf{E}(\mathbf{z})$ be a lossless system of order one in z_0*

$$\mathbf{E}(\mathbf{z}) = \sum_{n=0}^1 \sum_{n_1=0}^N \mathbf{e}(n_0, n_1) z_0^{-n_0} z_1^{-n_1}.$$

Then $\mathbf{E}(\mathbf{z})$ is of the form $\mathbf{E}(\mathbf{z}) = \mathbf{G}_0(z_0)\mathbf{F}(z_1)\mathbf{G}_1(z_0)$, where $\mathbf{F}(z_1)$, $\mathbf{G}_0(z_0)$ and $\mathbf{G}_1(z_0)$ are 1D FIR lossless systems.

By Theorem 8.2, $\mathbf{F}(z_1)$, $\mathbf{G}_0(z_0)$ and $\mathbf{G}_1(z_0)$ can be factorized into the 1D building block in (8.3). So the subclass of 2D FIR lossless systems that has order one in z_0 can be expressed as the product of the 1D building block in (8.3). Notice that there is no restriction on the order of z_1 .

Remark. Theorem 8.5 and Theorem 8.6 provide the necessary and sufficient conditions for the factorizability of 2D lossless systems. In Theorem 8.5, we see that a 2D lossless system $\mathbf{E}(\mathbf{z})$ can be factorized into systems of lower degrees in z_0 or z_1 if and only if $\mathbf{E}(\mathbf{z})$ admits a minimal first-level realization that satisfies those three conditions described in Theorem 8.5. However, there is no systematic approach to test whether $\mathbf{E}(\mathbf{z})$ admits such a first-level realization. Similarly, Theorem 8.6 states that a 2D lossless system $\mathbf{E}(\mathbf{z})$ can be factorized into systems of lower degrees in z_0 and z_1 if and only if $\mathbf{E}(\mathbf{z})$ admits a minimal Roesser realization that satisfies those three conditions described in Theorem 8.6. Again, there is no systematic approach to test whether $\mathbf{E}(\mathbf{z})$ admits such a Roesser realization.

Acknowledgements

Work supported in parts by NSF grant MIP 92-15785, Tektronix, Inc., and Rockwell International.

References

1. R. Ansari and C. Guillemot, "Exact reconstruction filter banks using diamond FIR filters," *Proc. Int. Conf. on New Trends in Comm. Control, and Signal Proc.*, Turkey, July 1990.
2. R. Ansari and C. L. Lau, "Two-dimensional IIR filters for exact reconstruction in tree-structured subband decomposition," *Electronic Letter*, vol. 23, June 1987, pp. 633-634.
3. R. H. Bamberg and M. J. T. Smith, "A filter bank for the directional decomposition of images: theory and design," *IEEE Trans. on Signal Processing*, vol. SP-40, no. 4, April 1992, pp. 882-893.

4. S. Basu, H. Choi, and C. Chiang, "On non-separable multidimensional perfect reconstruction filter banks," *Proc. of the 27th Annual Asilomar Conference on Signals, Systems and Computers*, 1993, pp. 45-49.
5. N. K. Bose, *Applied Multidimensional Systems Theory*, Van Nostrand Reinhold, 1982.
6. T. Chen and P. P. Vaidyanathan, "The role of integer matrices in multidimensional multirate systems," *IEEE Trans. on Signal Processing*, vol. SP-41, March 1993.
7. T. Chen and P. P. Vaidyanathan, "Recent developments in multidimensional multirate systems," *IEEE Trans. on Circuits And Systems For Video Technology*, vol. 3, no. 2, April 1993, pp. 116-137.
8. T. Chen and P. P. Vaidyanathan, "Consideration in multidimensional filter bank design," *Proc. International Symposium on Circuits and Systems*, May 1993.
9. T. Chen and P. P. Vaidyanathan, "Multidimensional multirate filters and filter banks derived from one dimensional filters," *IEEE Trans. on Signal Processing*, vol. SP-41, May 1993.
10. P. L. Chu, "Quadrature mirror filter design for an arbitrary number of equal bandwidth channels," *IEEE Trans. on Acoustic, Speech and Signal Processing*, vol. 33, Feb. 1985, pp. 203-218.
11. A. Cohen and I. Daubechies, "Nonseparable bidimensional wavelet bases," Preprint, 1993.
12. R. E. Crochiere, S. A. Waber, and J. L. Flanagan, "Digital coding of speech in subbands," *Bell Sys. Tech. Jour.*, vol. 55, Oct. 1976, pp. 1069-1085.
13. R. E. Crochiere and L. R. Rabiner, *Multirate Digital Signal Processing*, Englewood Cliffs: Prentice Hall, 1983.
14. Z. Doganata, P. P. Vaidyanathan, and T. Q. Nguyen, "General synthesis procedures for FIR lossless transfer matrices, for perfect-reconstruction multirate filter bank applications," *IEEE Trans. on Acoustic, Speech and Signal Processing*, vol. ASSP-36, Oct. 1988, pp. 1561-1574.
15. D. E. Dudgeon and R. M. Mersereau, *Multidimensional Digital Signal Processing*, Englewood Cliffs: Prentice Hall, 1984.
16. R. Eising, "Realization and stabilization of 2-D systems," *IEEE Trans. on Automatic Control*, vol. 23, Oct. 1978, pp. 793-799.
17. B. L. Evans, R. H. Bamberger, and J. H. McClellan, "Rules for multidimensional multirate structures," *IEEE Trans. on Signal Processing*, vol. SP-42, April 1994, pp. 762-771.
18. R. A. Gopinath and C. S. Burrus, "On upsampling, downsampling, and rational sampling rate filter banks," *IEEE Trans. on Signal Processing*, vol. SP-42, April 1994, pp. 812-824.
19. M. Ikehara, "Cosine-modulated 2 dimensional FIR filter banks satisfying perfect reconstruction," *Proc. International Conf. on Acoustic, Speech, and Signal Processing*, vol. III, April 1994, pp. 137-140.
20. M. Ikehara, "Modulated 2 dimensional perfect reconstruction FIR filter banks with permissible passbands," *Proc. International Conf. on Acoustic, Speech, and Signal Processing*, May 1995, pp. 1468-1471.
21. N. S. Jayant and P. Noll, *Digital Coding of Waveforms*, Englewood Cliffs: Prentice Hall, 1984.
22. A. A. C. M. Kalker, "Commutativity of up/down sampling," *Electron. Lett.*, vol. 28, no. 6, March 1992, pp. 567-569.
23. G. Karlsson and M. Vetterli, "Theory of two-dimensional multirate filter banks," *IEEE Trans. on Acoustic, Speech and Signal Processing*, vol. SP-38, June 1990, pp. 925-937.
24. C. W. Kim and R. Ansari, "FIR/IIR exact reconstruction filter banks with applications to subband coding of images," Midwest CAS Symposium, May 1991.
25. C. W. Kim and R. Ansari, "Subband decomposition procedure for quincunx sampling grids," *Proc. SPIE Visual Communications and Image Processing*, Boston, Nov. 1991.
26. R. D. Koilpillai and P. P. Vaidyanathan, "Cosine-modulated FIR filter banks satisfying perfect reconstruction," *IEEE Trans. on Signal Processing*, vol. 40, April 1992, pp. 770-783.
27. J. Kovacevic and M. Vetterli, "The commutativity of up/downsampling in two dimensions," *IEEE Trans. on Information Theory*, vol. 37, no. 4, May 1991, pp. 695-698.

28. J. Kovacevic and M. Vetterli, "Non-separable multidimensional perfect reconstruction filter banks and wavelet bases for R^n ," *IEEE Trans. on Information Theory*, vol. 38, no. 2, March 1992, pp. 533-555.
29. J. Kovacevic, "Local cosine bases in two dimensions," *Proc. International Conf. on Acoustic, Speech, and Signal Processing*, vol. IV, May 1995, pp. 2125-2128.
30. M. Kunt, A. Ikonopoulos and M. Kocher, "Second generation image coding techniques," *Proc. IEEE*, vol. 73, April 1985, pp. 549-574.
31. Y. Lin and P. P. Vaidyanathan, "Theory and design of two-dimensional cosine modulated filter banks," Tech. report, California Institute of Technology, Pasadena, CA, March 1995.
32. Y. Lin and P. P. Vaidyanathan, "Two-dimensional paraunitary cosine modulated perfect reconstruction filter banks," *Proc. International Symposium on Circuits and Systems*, April 1995, pp. 752-755.
33. Y. Lin and P. P. Vaidyanathan, "On the sampling of two-dimensional bandpass signal," In preparation.
34. V. C. Liu and P. P. Vaidyanathan, "On factorization of a subclass of 2D digital FIR lossless matrices for 2D QMF bank applications," *IEEE Trans. on Circuits and Systems*, vol. 37, no. 6, June 1990, pp. 852-854.
35. H. S. Malvar, *Signal Processing with Lapped Transforms*, Norwood, MA: Artech House, 1992.
36. J. H. McClellan, "The design of two-dimensional digital filters by transformations," *Proc. Seventh Annual Princeton Conf. Information Sciences and Systems*, 1973, pp. 247-251.
37. H. J. Nussbaumer, "Pseudo QMF filter bank," *IBM Tech. Disclosure Bulletin*, vol. 24, Nov. 1981, pp. 3081-3087.
38. S. Phoong, C. W. Kim, P. P. Vaidyanathan, and R. Ansari, "A new class of two-channel biorthogonal filter banks and wavelet bases," *IEEE Trans. on Signal Processing*, vol. SP-43, no. 3, March 1995, pp. 649-665.
39. T. A. Ramstad, "Cosine modulated analysis-synthesis filter bank with critical sampling and perfect reconstruction," *Proc. IEEE Int. Conf. Acoustic, Speech and Signal Processing*, Toronto, Canada, May 1991, pp. 1789-1792.
40. R. P. Roesser, "A discrete state-space model for linear image processing," *IEEE Trans. on Automatic Control*, vol. 20, Feb. 1975, pp. 1-10.
41. J. H. Rothweiler, "Polyphase quadrature filters, a new subband coding technique," *Proc. of the IEEE Int. Conf. on Acoustic, Speech and Signal Processing*, April 1973, pp. 1980-1983.
42. I. A. Shah and A. A. C. Kalker, "Generalized theory of multidimensional M-band filter bank design," *EUSIPCO*, 1992, pp. 969-972.
43. I. A. Shah and A. A. C. Kalker, "Algebraic theory of multidimensional filter banks and their design using transformations," preprint.
44. M. J. T. Smith and S. L. Eddins, "Analysis/synthesis techniques for subband image coding," *IEEE Trans. on Acoustic, Speech and Signal Processing*, vol. 38, no. 8, 1990, pp. 1446-1456.
45. D. B. H. Tay and N. G. Kingsbury, "Flexible design of multidimensional perfect reconstruction FIR 2-band filters using transformation of variables," *IEEE Trans. on Image Processing*, vol. 2, no. 4, Oct. 1993, pp. 466-480.
46. P. P. Vaidyanathan, "The discrete-time bounded-real lemma in digital filtering," *IEEE Trans. on Circuits and Systems*, vol. 32, Sept. 1985, pp. 918-924.
47. P. P. Vaidyanathan and T. Q. Nguyen, "A "Trick" for the design of FIR halfband filters," *IEEE Trans. on Circuits and Systems*, vol. 34, March 1987, pp. 297-300.
48. P. P. Vaidyanathan, "Fundamentals of multidimensional multirate digital signal processing," *Sadahana*, vol. 15, Nov. 1990, pp. 157-176.
49. P. P. Vaidyanathan, "New results in multidimensional multirate systems," *Proc. International Symposium on Circuits and Systems*, 1991, pp. 468-471.
50. P. P. Vaidyanathan, *Multirate Systems and Filter Banks*, Englewood Cliffs: Prentice Hall, 1993.
51. S. Venkataraman and B. C. Levy, "State space representations of 2D FIR lossless transfer matrices," *IEEE Trans. on Circuits and Systems*, vol. 41, Feb. 1994, pp. 117-131.

52. M. Vetterli, "Multidimensional subband coding: Some theory and algorithms," *Signal Processing*, vol. 6, no. 2, Feb. 1984, pp. 97-112.
53. E. Viscito and J. P. Allebach, "The analysis and design of multidimensional FIR perfect reconstruction filter banks for arbitrary sampling lattices," *IEEE Trans. on Circuits and Systems*, vol. CAS-38, no. 1, Jan. 1991, pp. 29-41.
54. J. W. Woods and S. D. O'Neil, "Subband coding of images," *IEEE Trans. on Acoust. Speech and Signal Proc.*, vol. 34, Oct. 1986, pp. 1278-1288.
55. J. W. Woods, *Subband Image Coding*, Norwell, MA: Kluwer Academic Publishers, Inc., 1991.
56. P. Yip, and K. R. Rao, "Fast discrete transforms," in *Handbook of Digital Signal Processing*, edited by D. F. Elliott, San Diego, CA: Academic Press, 1987.
57. D. C. Youla, "The synthesis of networks containing lumped and distributed elements," *Proc. Symp. on Generalized Networks*, New York: Polytechnic Institute of Brooklyn Press, Apr. 1966.

Selected References by Topic

Multidimensional Multirate Systems and Subband Coding

- [5] N. K. Bose, 1982.
- [52] M. Vetterli, 1984.
- [15] D. E. Dudgeon and R. M. Mersereau, 1984.
- [54] J. W. Woods and S. D. O'Neil, 1986.
- [23] G. Karlsson and M. Vetterli, 1990.
- [34] V. C. Liu and P. P. Vaidyanathan, 1990.
- [48] P. P. Vaidyanathan, 1990.
- [53] E. Viscito and J. P. Allebach, 1991.
- [27] J. Kovacevic and M. Vetterli, 1991.
- [55] J. W. Woods, 1991.
- [28] J. Kovacevic and M. Vetterli, 1992.
- [6] T. Chen and P. P. Vaidyanathan, 1993.
- [7] T. Chen and P. P. Vaidyanathan, 1993.
- [4] S. Basu, H. Choi, and C. Chiang, 1993.
- [50] P. P. Vaidyanathan, 1993.
- [51] S. Venkataraman and B. C. Levy, 1994.
- [17] B. L. Evans, R. H. Bamberger, and J. H. McClellan, 1994.
- [18] R. A. Gopinath and C. S. Burrus, 1994.

Two-Dimensional Two-channel Filter Bank Design

- [52] M. Vetterli, 1984.
- [2] R. Ansari and C. L. Lau, 1987.

Multidimensional Multirate Systems and Subband Coding

- [1] R. Ansari and C. Guillemot, 1990.
- [24] C. W. Kim and R. Ansari, 1991.
- [45] D. B. H. Tay and N. G. Kingsbury, 1993.
- [9] T. Chen and P. P. Vaidyanathan, 1993.
- [38] S. Phoong, C. W. Kim, P. P. Vaidyanathan, and R. Ansari, 1995.

Multidimensional Filter Bank Design

- [49] P. P. Vaidyanathan, 1991.
- [43] I. A. Shah and A. A. C. Kalker, 1992.
- [19] M. Ikehara, 1994.
- [32] Y. Lin and P. P. Vaidyanathan, 1995.
- [20] M. Ikehara, 1995.